Sigma1 receptors inhibit store-operated Ca²⁺ entry by attenuating coupling of STIM1 to Orai1

Shyam Srivats,[1] Dilshan Balasuriya,[1] Mathias Pasche,[2] Gerard Vistal,[1] J. Michael Edwardson,[1] Colin W. Taylor,[1] and Ruth D. Murrell-Lagnado[1,3]

[1]Department of Pharmacology, University of Cambridge, Cambridge CB2 1PD, England, UK
[2]MRC Laboratory for Molecular Biology, Cambridge CB2 0QH, England, UK
[3]Sussex Neuroscience, School of Life Sciences, University of Sussex, Brighton BN1 9QG, England, UK

Sigma1 receptors (σ1Rs) are expressed widely; they bind diverse ligands, including psychotropic drugs and steroids, regulate many ion channels, and are implicated in cancer and addiction. It is not known how σ1Rs exert such varied effects. We demonstrate that σ1Rs inhibit store-operated Ca²⁺ entry (SOCE), a major Ca²⁺ influx pathway, and reduce the Ca²⁺ content of the intracellular stores. SOCE was inhibited by expression of σ1R or an agonist of σ1R and enhanced by loss of σ1R or an antagonist. Within the endoplasmic reticulum (ER), σ1R associated with STIM1, the ER Ca²⁺ sensor that regulates SOCE. This interaction was modulated by σ1R ligands. After depletion of Ca²⁺ stores, σ1R accompanied STIM1 to ER–plasma membrane (PM) junctions where STIM1 stimulated opening of the Ca²⁺ channel, Orai1. The association of STIM1 with σ1R slowed the recruitment of STIM1 to ER–PM junctions and reduced binding of STIM1 to PM Orai1. We conclude that σ1R attenuates STIM1 coupling to Orai1 and thereby inhibits SOCE.

Introduction

Sigma1 receptors (σ1Rs) are widely distributed in the brain and peripheral tissues, including lung, kidney, liver, and spleen, and highly expressed in some tumor cells (Walker et al., 1990; Vilner et al., 1995; Monnet, 2005; Stone et al., 2006; Cobos et al., 2008; Wu and Bowen, 2008; Su et al., 2010; Brune et al., 2013). They are regulated by an unusually diverse array of ligands, including endogenous steroids, drugs of abuse such as cocaine and methamphetamine, and drugs used to treat depression, anxiety, psychosis, pain, and neurodegenerative diseases (Maurice et al., 1999; Waterhouse et al., 2007; Maurice and Su, 2009; Su et al., 2010; Navarro et al., 2012; Robson et al., 2012; Wünsch, 2012; Kourrich et al., 2013; Tsai et al., 2014). Changes in expression and polymorphisms of σ1Rs are associated with heart failure (Ito et al., 2012, 2013), addiction (Maurice et al., 2002; Kourrich et al., 2013), neurodegenerative and psychiatric disorders (Miki et al., 2014; Tsai et al., 2014), and cancer (Spruce et al., 2004; Wang et al., 2004; Aydar et al., 2006; Maurice and Su, 2009; Crottès et al., 2013). These associations have provoked interest in σ1Rs as both therapeutic targets and diagnostic tools (van Waarde et al., 2015).

The σ1R is an integral membrane protein with two transmembrane domains. It is expressed in the ER, where it is concentrated in cholesterol-rich mitochondrion-associated ER membrane (MAM) domains and bound to the ER luminal chaperone, BiP (Fig. S1; Hayashi and Su, 2003, 2007; Palmer et al., 2007). Agonists of σ1R cause it to dissociate from BiP and MAM, allowing σ1Rs to move within ER membranes and interact with signaling proteins in the plasma membrane (PM), most notably ion channels, thereby regulating their activity (Su et al., 2010; Balasuriya et al., 2012; Pabba, 2013). Antagonists block this effect (Fig. S1 and Table S1). Loss of Ca²⁺ from the ER can also release σ1Rs from their interaction with BiP, freeing them to interact with other proteins (Hayashi and Su, 2007). In addition to regulating the activity of these proteins, σ1Rs can also act as chaperones, stabilizing signaling proteins as they traffic along the secretory pathway (Tsai et al., 2014). σ1Rs may also be expressed in the nuclear envelope (Hayashi and Su, 2005a,b; Brune et al., 2013; Mori et al., 2013) and PM (Lupardus et al., 2000; Aydar et al., 2002; Brune et al., 2013; Balasuriya et al., 2014a) and may even be secreted into the extracellular space (Hayashi and Su, 2003; Su et al., 2010). The interactions between σ1Rs and ion channels may therefore occur within the plane of a membrane (ER or PM) or across ER–PM junctions (Hayashi and Su, 2007; Kourrich et al., 2013; Balasuriya et al., 2014a). Clearly, σ1Rs are important links between diverse ligands, physiological stimuli, and many key signaling molecules (Hayashi and Su, 2007; Su et al., 2010; Kourrich et al., 2013).

The Rockefeller University Press $30.00
J. Cell Biol. Vol. 213 No. 1 65–79
www.jcb.org/cgi/doi/10.1083/jcb.201506022

JCB 65

THE JOURNAL OF CELL BIOLOGY

Receptors that stimulate PLC and formation of inositol 1,4,5-trisphosphate (IP$_3$) evoke both Ca^{2+} release from the ER through IP$_3$ receptors (IP$_3$Rs) and Ca^{2+} entry across the PM. At MAMs, Ca^{2+} released by IP$_3$Rs can be rapidly accumulated by mitochondria, thereby stimulating oxidative phosphorylation (Rizzuto et al., 2012) and promoting cell survival (Cárdenas et al., 2010), whereas excessive mitochondrial Ca^{2+} uptake triggers apoptosis (Mallilankaraman et al., 2012). The association of IP$_3$R3s with σ1Rs at MAMs supports the transfer of Ca^{2+} from the ER to mitochondria by curtailing the degradation of active IP$_3$R3s (Hayashi and Su, 2007). The increase in mitochondrial Ca^{2+} concentration and resultant boost in oxidative phosphorylation are thought to contribute to the prosurvival effects of σ1Rs in the central nervous system and cancer cells (Lewis et al., 2014). One effect of σ1Rs may therefore be to support transfer of Ca^{2+} from the ER to mitochondria, but this transfer also depends on the Ca^{2+} content of the ER.

The Ca^{2+} entry evoked by receptors that stimulate PLC is usually mediated by store-operated Ca^{2+} entry (SOCE), which is stimulated by loss of Ca^{2+} from the ER (Parekh and Putney, 2005; Hogan and Rao, 2015). The reduction in Ca^{2+} concentration within the ER is detected by the luminal EF hands of stromal interaction molecule 1 (STIM1), an integral ER membrane protein. This causes STIM1 to cluster and accumulate at ER–PM junctions. STIM1 then binds to Orai1, a Ca^{2+}-permeable channel in the PM, and activates it (Lewis, 2007; Soboloff et al., 2012; Wu et al., 2014). The contributions of related proteins (Orai2, Orai3, and STIM2) to SOCE are not fully resolved (Hoth and Niemeyer, 2013), although STIM2 is usually more important than STIM1 for refilling of Ca^{2+} stores (Brandman et al., 2007). Additional proteins, including junctate, CRACR2, and SOCE-associated regulatory factor (SARAF), also interact with STIM1–Orai1 signaling complexes and regulate both activation and deactivation of SOCE (Srikanth et al., 2010, 2012, 2013; Palty et al., 2012; Srikanth and Gwack, 2012, 2013).

We show that σ1Rs constitutively inhibit SOCE and reduce the Ca^{2+} content of the ER and that σ1R ligands modulate this inhibition. The σ1R associates with STIM1 in the ER and is conveyed with STIM1 to ER–PM junctions after store depletion. This association slows the recruitment of STIM1 to the junctions and reduces binding of STIM1 to Orai1. Our results establish that σ1Rs inhibit a ubiquitous Ca^{2+} entry pathway and suggest a general model for directed translocation of σ1R to its PM targets.

Results

σ1R inhibits SOCE

SOCE in human embryonic kidney (HEK) cells can be activated by depletion of intracellular Ca^{2+} stores using thapsigargin to inhibit the ER Ca^{2+} pump or by stimuli of endogenous receptors (e.g., ATP or carbachol) that activate PLC. The contributions of Orai1 and STIM1 to SOCE (Parekh and Putney, 2005; DeHaven et al., 2009; Soboloff et al., 2012) are clear from the inhibition of thapsigargin-evoked Ca^{2+} entry in HEK cells expressing a dominant-negative form of Orai1 (Orai1^{E106Q}; Prakriya et al., 2006) and the enhancement of SOCE after overexpression of Orai1 with STIM1 (Fig. 1, A and B). The initial Ca^{2+} release evoked by thapsigargin was unaffected by these effects of Orai1 and STIM on SOCE. Stable expression of a V5-tagged σ1R in HEK cells (HEK-σ1R cells) attenuated the Ca^{2+} signals

evoked by thapsigargin without affecting expression of Orai1 or STIM1 (103 ± 5% and 91 ± 8% of wild-type cells, respectively; Fig. 1 C) or the basal cytosolic free Ca^{2+} concentration ([Ca^{2+}]$_c$; 45 ± 7 nM and 50 ± 3 nM in wild-type and HEK-σ1R cells, respectively). The increase in [Ca^{2+}]$_c$ after addition of thapsigargin in Ca^{2+}-free medium was reduced by 65 ± 9%, and the SOCE detected after restoration of extracellular Ca^{2+} was reduced by 86 ± 4% in HEK-σ1R cells (Fig. 1, D and E). The rate of increase of [Ca^{2+}]$_c$ during SOCE decreased from 8.8 ± 0.3 nM.s^{-1} in wild-type HEK cells to 2.8 ± 0.3 nM.s^{-1} in HEK-σ1R cells. SOCE in HEK-σ1R cells was similarly reduced across a range of extracellular Ca^{2+} concentrations (Fig. S2 A). The inhibition of both thapsigargin-evoked Ca^{2+} release and SOCE in HEK-σ1R cells was also observed at 37°C (Fig. S2 B) and in single-cell measurements (Fig. 1 F). The diminished SOCE did not result from ineffective store emptying because it was unaffected by prolonging the incubation with thapsigargin from 10 to 20 min (Fig. 1 E). Indeed, both the initial Ca^{2+} content of the stores (determined by addition of ionomycin in Ca^{2+}-free medium, the effects of which are not restricted to the ER) and the residual content after thapsigargin treatment were reduced in HEK-σ1R cells (Fig. 1, G and H). When ATP and carbachol were used to deplete Ca^{2+} stores via endogenous pathways, the Ca^{2+} release and Ca^{2+} entry were also attenuated in HEK-σ1R cells (Fig. 1, I and J). The lesser Ca^{2+} release evoked by ATP and carbachol in HEK-σ1R cells (52 ± 8% of wild-type cells) matched the reduced Ca^{2+} content of the stores (59 ± 9%), suggesting that this was responsible for the diminished response to PLC-coupled receptors.

To investigate whether sustained depletion of Ca^{2+} stores might itself cause down-regulation of SOCE, HEK cells were treated with cyclopiazonic acid (CPA) to reversibly inhibit the ER Ca^{2+} pump for a 2-h period that later experiments (see Fig. 3) show is sufficient for σ1R agonists to inhibit SOCE. This CPA treatment caused a more substantial depletion of the intracellular Ca^{2+} stores than was observed in HEK-σ1R cells, but a much smaller inhibition of the SOCE evoked by subsequent addition of thapsigargin (Fig. 2, A and B). These results establish that loss of Ca^{2+} from the ER does not cause the reduced SOCE in HEK-σ1R cells.

The smaller increase in [Ca^{2+}]$_c$ evoked by SOCE in HEK-σ1R cells could result from decreased Ca^{2+} entry or enhanced Ca^{2+} extrusion. However, rates of recovery from Ca^{2+} signals evoked by carbachol and ATP in Ca^{2+}-free medium (measured over matched [Ca^{2+}]$_c$) were unaffected by expression of σ1R (half-times, t$_{1/2}$ = 36 ± 5 s and 32 ± 6 s for wild-type and HEK-σ1R cells, respectively). The smaller [Ca^{2+}]$_c$ increases in HEK-σ1R cells were not, therefore, due to more effective buffering or Ca^{2+} extrusion. Because most Ca^{2+} extrusion pathways do not transport Mn^{2+}, we used quenching of fura 2 fluorescence to measure unidirectional Mn^{2+} influx through the SOCE pathway (Fig. 2 C). Thapsigargin, or carbachol with ATP, stimulated Mn^{2+} entry in HEK cells, consistent with the activation of SOCE in response to store depletion. In HEK-σ1R cells, there was no change in the rate of Mn^{2+} entry in response to either stimulus (Fig. 2 D). Together, these results establish that stable expression of σ1R inhibits SOCE.

Selection of polyclonal HEK cells stably expressing σ1R might have propagated cells with different Ca^{2+} signaling behaviors. However, the thapsigargin-evoked increase in [Ca^{2+}]$_c$ and SOCE and the Ca^{2+} content of the intracellular stores were also reduced in HEK cells transiently expressing σ1Rs (Fig. S2,
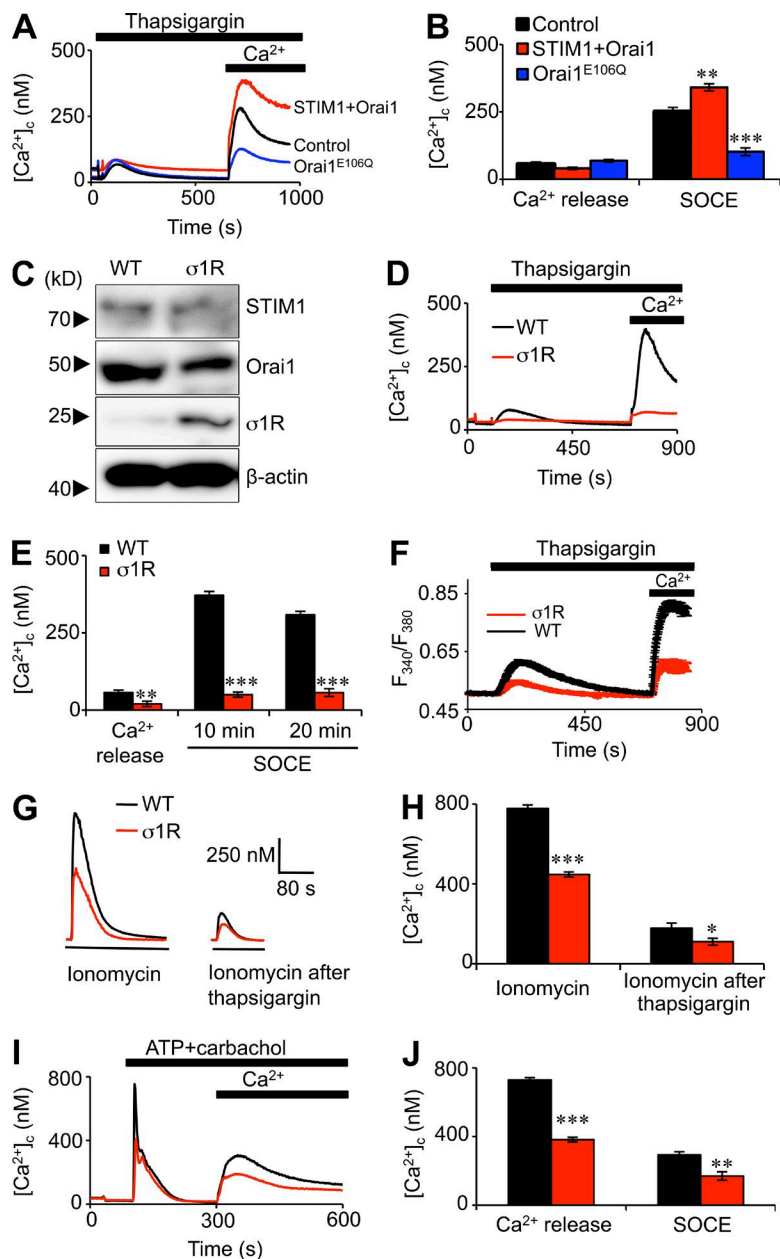
Figure 1. **Inhibition of SOCE by σ1R.** (A) Ca^{2+} signals recorded from populations of fluo 4–loaded HEK cells transiently transfected with $Orai1^{E106Q}$, STIM1 and Orai1, or mock transfected (control). Cells were stimulated with 5 µM thapsigargin in Ca^{2+}-free HBS before restoration of extracellular Ca^{2+} (final free $[Ca^{2+}]$, 4 mM). Results show mean responses from six replicates. (B) Summary results ($n = 3$) show peak increases in $[Ca^{2+}]_c$ evoked by thapsigargin (Ca^{2+} release) and Ca^{2+} restoration (SOCE). (C) Typical immunoblot of σ1R, STIM1, Orai1, and β-actin from 20 µg of solubilized protein from wild-type (WT) HEK and HEK-σ1R cells. (D) Ca^{2+} signals evoked by thapsigargin in Ca^{2+}-free HBS and after restoration of extracellular Ca^{2+} to wild-type and HEK-σ1R cells. (E) Summary shows responses to thapsigargin (Ca^{2+} release) and SOCE detected after restoring Ca^{2+} 10 or 20 min after thapsigargin ($n = 6$). (F) Responses from single fura 2–loaded HEK cells show fluorescence ratios (F_{340}/F_{380}) after stimulation with 5 µM thapsigargin and restoration of 4 mM extracellular Ca^{2+}. $n = 3$, each with ~45 cells. (G) Ca^{2+} contents of the intracellular stores determined by measuring $[Ca^{2+}]_c$ after addition of 5 µM ionomycin in Ca^{2+}-free HBS before or 10 min after treatment with thapsigargin. (H) Summary results ($n = 6$). (I) Ca^{2+} release and SOCE evoked by 100 µM carbachol and 100 µM ATP. (J) Summary results ($n = 6$). *, P < 0.05; **, P < 0.01; ***, P < 0.001. Student's t test (E, H, and J) or ANOVA with Tukey's posthoc analysis (B). Results show mean ± SEM.

C–E). The reduced SOCE correlated with the level of expression of σ1R (Fig. S2, F and G). Translocation of GFP-tagged nuclear factor of activated T cells (NFAT) from the cytosol to the nucleus requires SOCE (Kar et al., 2011). SOCE stimulated NFAT translocation in HEK cells, and the response was attenuated to similar degrees in cells stably or transiently expressing σ1R (Fig. 2, E and F).

We conclude that expression of σ1R inhibits SOCE by reducing the coupling of empty stores to the activation of SOCE.

Agonists and antagonists of σ1R regulate SOCE

The σ1R agonist (+)SKF10047 (Su et al., 2010; Navarro et al., 2012) and the antagonist BD1047 (Fig. S1; Skuza and Rogóz, 2006; Gromek et al., 2014) were used to investigate the acute effects of σ1Rs in CHO cells and HEK-σ1R cells. In CHO cells, σ1Rs are endogenously expressed (Hayashi and Su, 2007). As in HEK cells, SOCE was inhibited by transient expression of

$Orai1^{E106Q}$, although in CHO cells, the thapsigargin-evoked Ca^{2+} release was also inhibited (Fig. S3 A). In both CHO and HEK-σ1R cells, preincubation with BD1047 increased the amplitude of the Ca^{2+} signals evoked by SOCE, whereas the agonist (+)SKF10047 had the opposite effect (Fig. 3, A–D). Neither ligand affected SOCE in wild-type HEK cells (Fig. 3, E and F), confirming that the effects are mediated by σ1Rs. The temperature dependence and slow equilibration of ligand binding to σ1Rs (Yamamoto et al., 2001; Chu and Ruoho, 2016), together with the need to load cells with Ca^{2+} indicators at 20°C, limited opportunities to investigate the time course of the effects of σ1R ligands. Nevertheless, it is clear that treatment with ligands for at least 1 h at 37°C before loading cells with Ca^{2+} indicator (1.5 h) in the continued presence of ligands was required to detect significant effects of the ligands on SOCE (Fig. S3, B–D).

In CHO cells, siRNA to σ1R almost abolished expression of endogenous σ1R, but this was accompanied by reduced expression of Orai1 and increased expression of STIM1 (Fig. 3, G
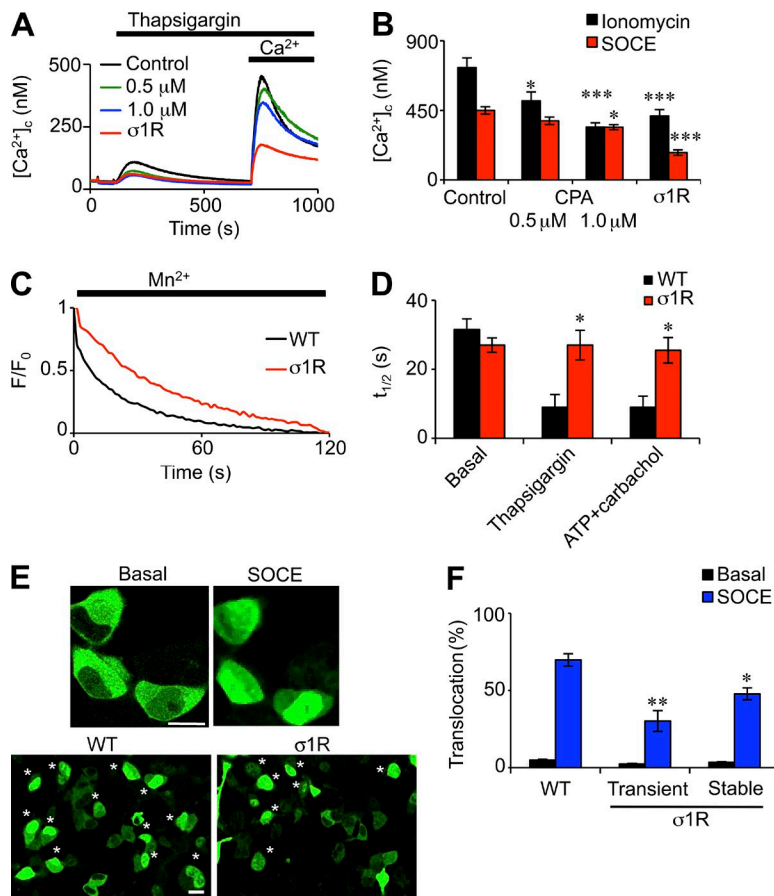
Figure 2. Stable and transient expression of σ1R inhibits SOCE. (A) Ca^{2+} signals evoked by 1 µM thapsigargin in Ca^{2+}-free HBS followed by restoration of 4 mM extracellular Ca^{2+} in HEK wild-type cells treated with CPA (0.5 µM or 1 µM for 2.5 h) or HEK-σ1R cells. (B) Summary results show peak increases in $[Ca^{2+}]_c$ evoked by SOCE or by addition of ionomycin in Ca^{2+}-free HBS ($n = 3$). (C) Populations of fura 2–loaded cells were treated with thapsigargin (5 µM for 10 min) in nominally Ca^{2+}-free HBS before addition of 5 mM $MnCl_2$. Results show normalized fluorescence intensity (F/F_0) for six replicates. WT, wild type. (D) Summary results ($n = 3$) show half-times ($t_{1/2}$) for fluorescence quenching from unstimulated cells (basal) and cells treated with thapsigargin (5 µM for 10 min) or ATP and carbachol (100 µM each for 3.5 min). (E) Typical images of HEK cells expressing NFAT-GFP before and 30 min after addition of 5 µM thapsigargin in normal HBS (top). Bar, 10 µm. Images of larger fields (bottom) show thapsigargin-treated HEK wild-type and HEK-σ1R cells. Asterisks indicate cells used for analysis. Bar, 20 µm. (F) Summary results show nuclear translocation of NFAT-GFP before and after treatment with thapsigargin (percentage of cells; six independent fields, with between 595 and 660 cells counted for each condition). *, $P < 0.05$; **, $P < 0.01$; ***, $P < 0.001$. Student's t test (D) or ANOVA with Tukey's posthoc analysis (B and F). Results show mean ± SEM.

and H). The loss of Orai1 could reflect a chaperone role for σ1R similar to the stabilization of human ether-a-go-go–related gene (HERG) K^+ channels by σ1R (Hayashi and Su, 2007; Crottès et al., 2011). Alternatively, Orai1 expression may be down-regulated through an adaptive feedback mechanism arising from the reduced inhibition of SOCE after loss of σ1Rs. Over-stimulation of SOCE by constitutively active STIM1 was shown previously to reduce Orai1 expression (Kilch et al., 2013). Despite the reduced expression of Orai1, SOCE was increased in CHO cells lacking σ1Rs, and it was then unaffected by (+)SKF10047 or BD1047 (Fig. 3, I and J). The enhanced SOCE in CHO cells lacking σ1Rs was abolished by expression of the dominant-negative form of Orai1 (Fig. S3 G), confirming that it was mediated by Orai1. SOCE monitored by unidirectional Mn^{2+} entry was also increased in CHO cells treated with siRNA to σ1R (Fig. S3, E and F). In normal CHO cells, (+)SKF10047 reduced the Ca^{2+} content of the stores, whereas the σ1R antagonist BD1047 increased their content to a level that matched that of cells without σ1Rs. Neither ligand affected the Ca^{2+} stores in CHO cells lacking σ1Rs (Fig. 3, K and L). Although comparison of SOCE-mediated Ca^{2+} signals in CHO cells with and without σ1Rs is compromised by accompanying changes in STIM1 and Orai1 expression (Fig. 3, G and H), the analyses demonstrate that σ1R ligands are effective only in cells expressing σ1Rs, and they establish a constitutive inhibition of SOCE by endogenous σ1Rs and an associated reduction in ER Ca^{2+} content in CHO cells (Fig. 3, I-L). Similar results were obtained in HEK-σ1R cells: siRNA to σ1R abolished the effects of σ1R ligands on both SOCE and the Ca^{2+} content of the stores; it also increased the basal Ca^{2+} content of the stores and the rate of

Mn^{2+} entry evoked by either thapsigargin or by the more physiological stimuli, ATP and carbachol (Fig. S3, H and J).

Determining whether ligands of σ1R are more effective before or after depletion of Ca^{2+} stores was frustrated by the need for prolonged preincubations at 37°C for optimal effects (Fig. S3, B–D). In a modified protocol, fluo 4–loaded HEK-σ1R cells in Ca^{2+}-free Hepes-buffered saline (HBS) were incubated with (+)SKF10047 or BD1047 for 2 h at 20°C, with thapsigargin added either immediately before the ligands or after the 2-h incubation. Under these conditions, where the effects of the ligands were much reduced, (+)SKF10047 modestly inhibited SOCE, and BD1047 modestly enhanced SOCE, but only when added before store depletion (Fig. S3 K). These results suggest that σ1R ligands affect an early step in the activation of SOCE.

Breast cancer cells express high levels of σ1Rs (Spruce et al., 2004; Wang et al., 2004; Aydar et al., 2006). In MDA-MB-231 human breast cancer cells, which also express σ1Rs, SOCE was enhanced by BD1047 and inhibited by (+)SKF10047 (Fig. S4). The Ca^{2+} content of the stores was also reduced by (+)SKF10047. Hence, in three cell types, HEK-σ1R, CHO, and MDA-MB-231 cells, σ1Rs both inhibit SOCE and decrease the Ca^{2+} content of the ER. The inverse agonist effect of BD1047 in CHO and MDA-MB-231 cells suggests a constitutive regulation of SOCE and ER Ca^{2+} content by endogenous σ1Rs.

σ1R and STIM1 associate and move to ER–PM junctions after store depletion

Interactions between σ1R and STIM1 in unstimulated cells were investigated using HEK cells transiently expressing STIM1-Myc and σ1R-FLAG. Anti-Myc beads pulled down σ1R-FLAG
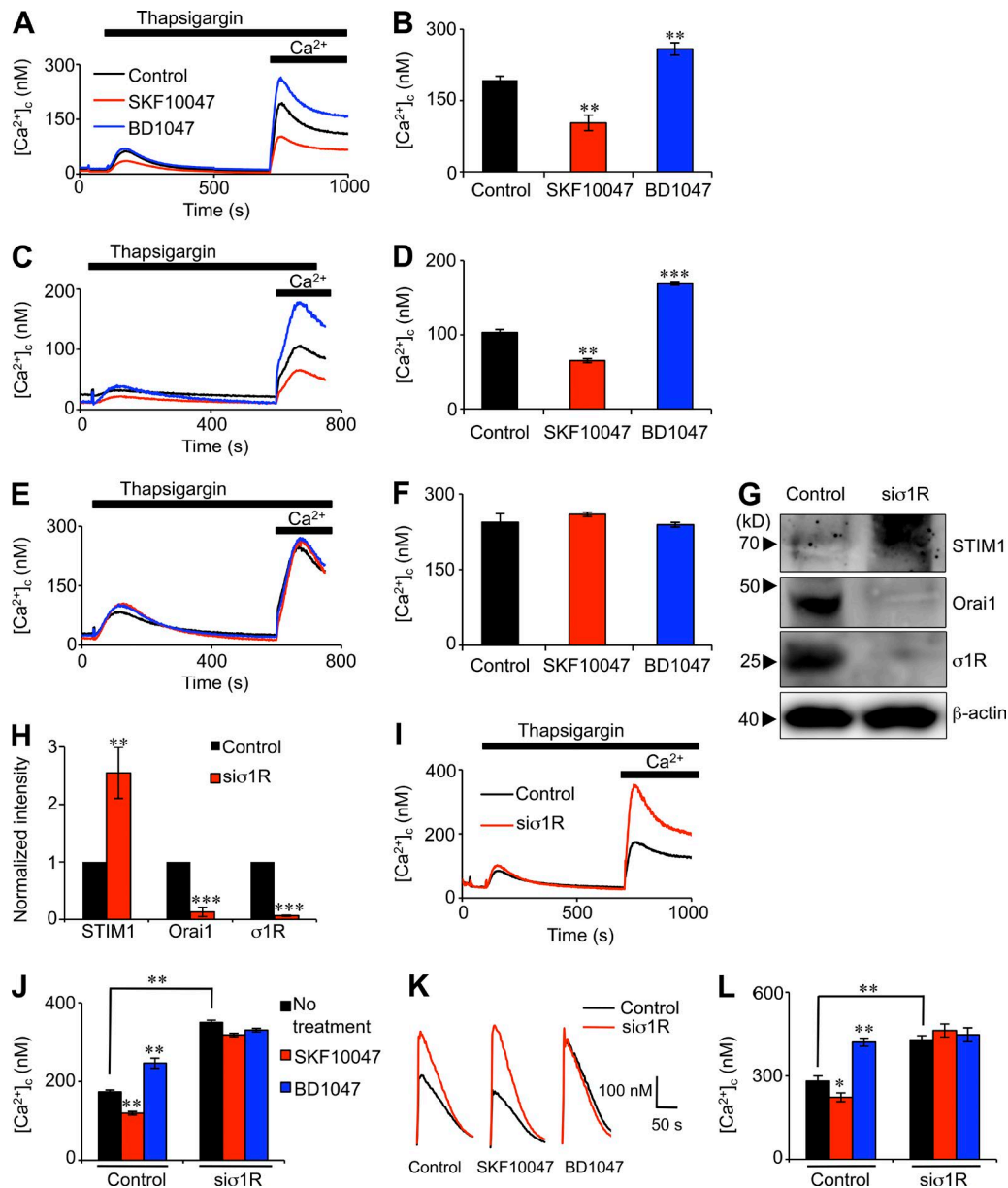
Figure 3. **Ligands of σ1R modulate SOCE.** (A–F) Populations of cells were treated with 25 μM (+)SKF10047 or 10 μM BD1047 before removal of extracellular Ca^{2+}, addition of 5 μM thapsigargin, and then restoration of extracellular 4 mM Ca^{2+} to CHO (A and B), HEK-σ1R (C and D), or wild-type HEK cells (E and F). Summary results (B, D, and F) show peak increases in $[Ca^{2+}]_c$ after restoration of extracellular Ca^{2+}. The color codes in A apply to all panels (A–F). (G) Representative immunoblot from CHO cells transfected with control plasmid or plasmid encoding siRNA for σ1R (siσ1R). (H) Summary results show band intensities for the indicated proteins normalized to those from cells treated with control plasmid. (I) Ca^{2+} signals evoked by addition of thapsigargin in Ca^{2+}-free HBS and then restoration of extracellular Ca^{2+} in CHO cells treated with siσ1R or control plasmid. (J) Summary shows peak $[Ca^{2+}]_c$ after restoration of extracellular Ca^{2+} to thapsigargin-treated CHO cells treated with siσ1R or control plasmid. Cells were pretreated with 25 μM (+) SKF10047 or 10 μM BD1047, as indicated. (K and L) Effects of siσ1R or control plasmid and pretreatment with σ1R ligands on the Ca^{2+} signals evoked by 5 μM ionomycin in Ca^{2+}-free HBS. Typical traces (K) and summary results (L) are shown. Legends for L are the same as J. All summary results show mean ± SEM. *n* = 3. *, P < 0.05; **, P < 0.01; ***, P < 0.001. ANOVA with Tukey's posthoc analysis (B, D, F, J, and L) or Student's *t* test (H and comparison of no treatment conditions in J and L).

from solubilized cell extracts, but only in cells expressing STIM1-Myc. Conversely, anti-FLAG beads pulled down STIM1-Myc, but only in cells expressing σ1R-FLAG (Fig. 4, A and B). Coimmunoprecipitation of σ1R-FLAG with STIM1-Myc was enhanced by (+)SKF10047 and reduced by BD1047 (Fig. 4, C–E). These results show that STIM1 and σ1R are associated in unstimulated cells and that their interaction is regulated by σ1R ligands. Furthermore, the increased association

of σ1R with STIM1 evoked by the σ1R agonist (Fig. 4) correlates with the inhibition of SOCE (Fig. 3).

To investigate the intracellular dynamics of σ1R and STIM1, we used HeLa cells because they are better suited than HEK cells for optical analyses of ER proteins while still lacking detectable endogenous σ1Rs (Fig. 5 A). In cells expressing σ1R-EGFP with mCh-STIM1, σ1R-EGFP and mCh-STIM1 colocalized within the ER (Mander's correlation coefficient
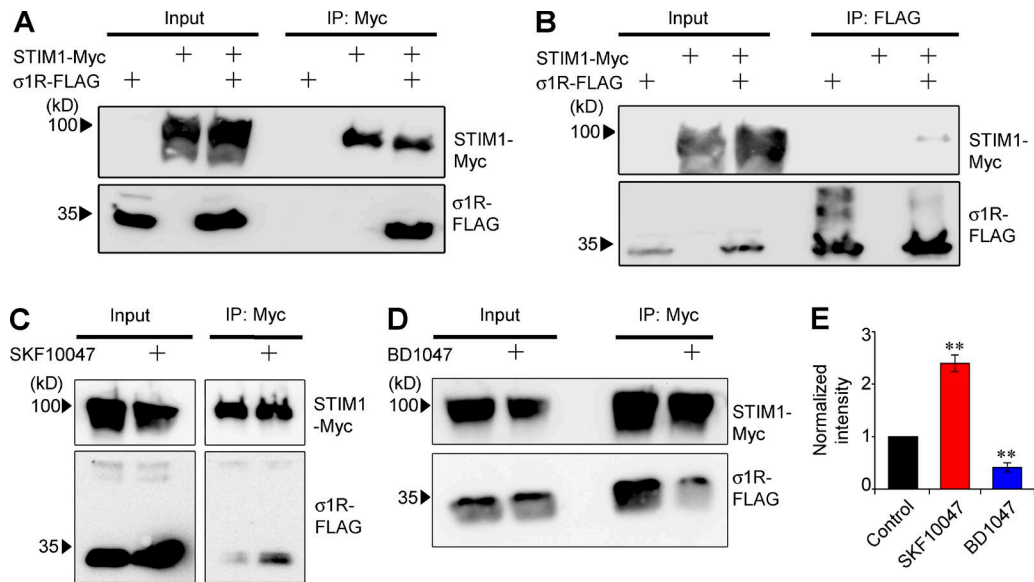
Figure 4. **Ligands regulate association of σ1R with STIM1.** (A and B) Solubilized HEK cells expressing STIM1-Myc, σ1R-FLAG, or both were immunoprecipitated (IP) with anti-Myc (A) or anti-FLAG (B) antibodies before immunoblotting. Input lanes were loaded with 10 µl of the 500-µl sample and immunoprecipitation lanes with 20 µl of the 50-µl eluate. (C and D) Similar immunoprecipitation analyses from cells expressing STIM1-Myc and σ1R-FLAG after pretreatment with 25 µM (+)SKF10047 or 10 µM BD1047. (E) Summary results (normalized to control cells; mean ± SEM; n = 3) show amounts of σ1R-FLAG immunoprecipitated by anti-Myc antibody in cells transiently expressing STIM1-Myc and σ1R-FLAG. **, P < 0.01. ANOVA with Tukey's posthoc analysis.

was 0.77 ± 0.03; $n = 8$; Fig. 5 B). We used total internal reflection fluorescence (TIRF) microscopy to visualize translocation of mCh-STIM1 and σ1R-EGFP in response to thapsigargin. In cells expressing mCh-STIM1, thapsigargin stimulated an accumulation of mCh-STIM1 in puncta immediately beneath the PM (Fig. 5 C, top). This is consistent with evidence that store depletion causes STIM1 to aggregate into sub-PM clusters, where they interact with Orai1 to activate SOCE (Liou et al., 2007; Wu et al., 2014). In contrast, thapsigargin had no detectable effect on the sub-PM distribution of σ1R-EGFP expressed alone (Fig. 5 C, bottom). However, when mCh-STIM1 and σ1R-EGFP were coexpressed, thapsigargin caused both proteins to accumulate in sub-PM puncta, within which the proteins colocalized (Mander's correlation coefficient was 0.77 ± 0.04; $n = 8$; Fig. 5 D), but expression of σ1R slowed the rate of formation of the mCh-STIM1 puncta (Fig. 5 E). Rates of formation of mCh-STIM1 puncta were unaffected by expression of another ER membrane protein, IP$_3$R1 (times to 50% accumulation were 325 ± 14 s and 342 ± 11 s, with and without IP$_3$R1, respectively), confirming that the effects of σ1R were not caused by nonspecific accumulation of ER proteins. Furthermore, in cells coexpressing Orai1-EGFP, σ1R-mKate, and HA-STIM1, Orai1-EGFP and σ1R-mKate accumulated into colocalized puncta after thapsigargin treatment, but neither formed puncta in the absence of STIM1 (Fig. 5, F and G). These results demonstrate that after store depletion, σ1R accompanies STIM1 to ER–PM junctions, but σ1R slows the accumulation of STIM1.

In related experiments, HeLa cells expressing different combinations of σ1R-EGFP, mCh-STIM1, and Orai1-Myc were fixed for immunolabeling, and confocal images were analyzed to assess colocalization of the proteins before and after treatment with thapsigargin. As expected, in cells coexpressing STIM1 and Orai1, thapsigargin caused their colocalization to increase, consistent with evidence that clustered STIM1 at ER–PM junctions captures Orai1 as it diffuses within the PM (Wu et al., 2014). In contrast, when σ1R and Orai1 were coexpressed,

their colocalization was enhanced by store depletion only in the presence of STIM1, and overlapping puncta of all three proteins were then apparent at the cell periphery (Fig. 5, H and I). These results agree with those obtained using TIRF microscopy and demonstrate the importance of STIM1 in recruiting both Orai1 and σ1R to the same junctions.

σ1R reduces the association of STIM1 with PM Orai1

The requirement for STIM1 in recruiting σ1R to ER–PM junctions containing Orai1 was investigated further by expressing σ1R-FLAG and Orai1-Myc with and without HA-STIM1. After treatment with thapsigargin and cell surface biotinylation, PM protein complexes were purified using avidin. Immunoblotting showed that the amount of σ1R within the biotinylated sample was significantly increased in cells overexpressing STIM1 and Orai1, but not when only Orai1 was overexpressed (Fig. 6, A and B). This indicates that STIM1 either promotes trafficking of σ1R to the PM, where it is directly biotinylated, or it promotes association of σ1R with a biotinylated PM protein. Similar analyses established that expression of σ1R-FLAG reduced the amount of STIM1 in the biotinylated sample to $47 \pm 12\%$ ($n = 3$) of that measured without σ1R (Fig. 6, C and D). The β-actin control showed no evidence of cell permeabilization or biotinylation of intracellular proteins. The biotinylated PM sample was subjected to a further round of purification using anti-Myc beads. Immunoblotting confirmed that when all three proteins were expressed, they were each captured in the final extract, suggesting that both STIM1 and σ1R are associated with the PM Orai1 channel complex (and that there is no need to invoke cell surface expression of σ1R to account for its presence in the biotinylated sample). The amount of STIM1 within this complex was again reduced by σ1R to $51 \pm 7\%$ of that measured without σ1R (Fig. 6, C and D). These results indicate that σ1R reduces the amount of STIM1 bound to PM Orai1. This was confirmed by purifying HA-STIM1 with anti-HA beads:
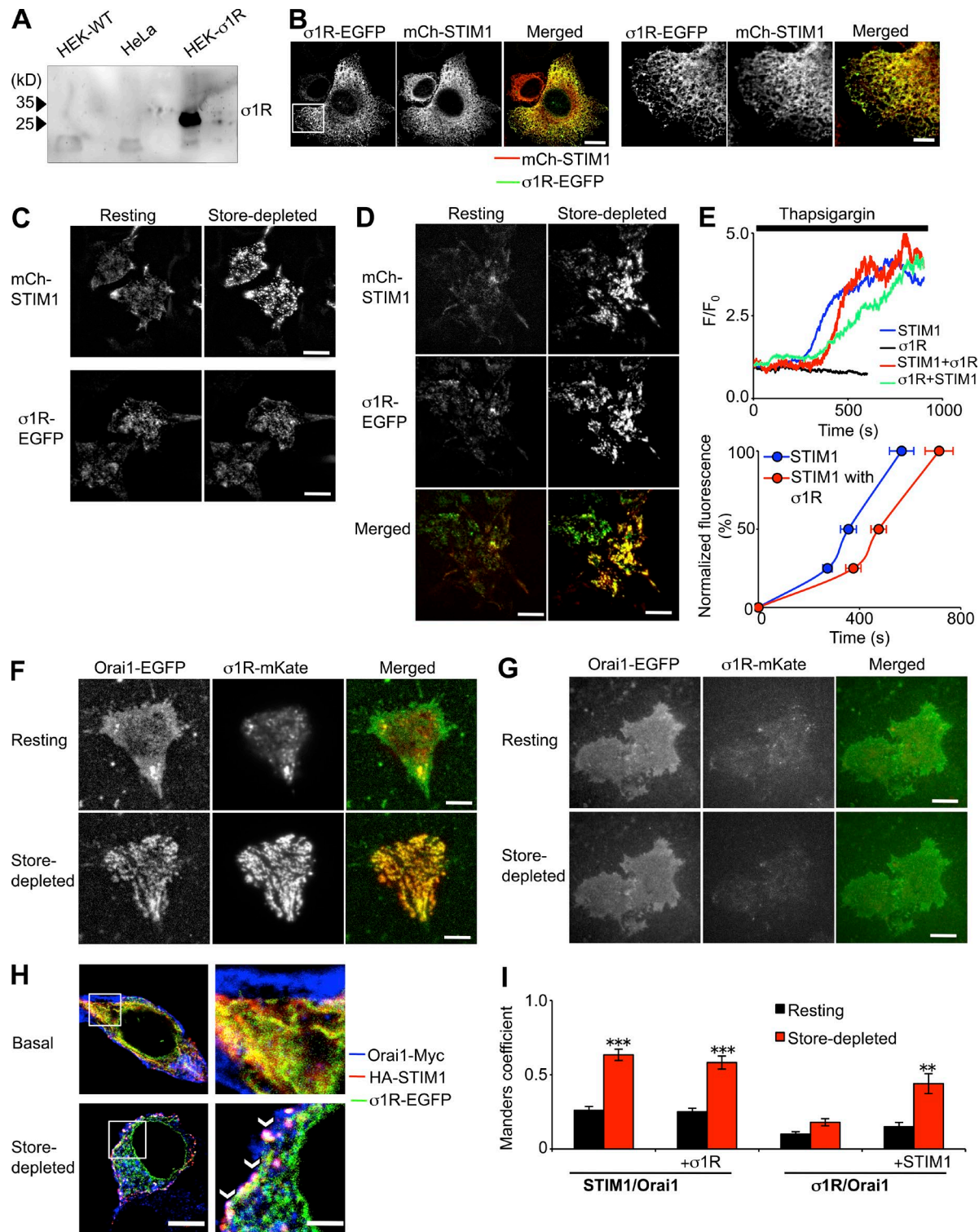
Figure 5. **σ1R accompanies STIM1 to ER–PM junctions after store depletion.** (A) Immunoblot of lysates from wild-type (WT) HEK, HEK-σ1R, or HeLa cells. The same amount of protein was loaded in each lane. (B) Confocal images of unstimulated HeLa cells transiently transfected with σ1R-EGFP and mCh-STIM1. Bar, 10 μm. (Right) Enlargement of the boxed area. Bar, 2.5 μm. (C and D) TIRF images of HeLa cells expressing mCh-STIM1 (C, top), σ1R-EGFP (C, bottom), or both (D) before and 10 min after addition of 5 μM thapsigargin in Ca^{2+}-free HBS. (E, top) Traces show time courses of the fluorescence changes (F/F_0) within the TIRF field after addition of thapsigargin (mean values for 30 puncta for each or size-matched regions of interest for σ1R alone). (E, bottom) Summary results show changes in mCh fluorescence (normalized to maximal intensity) after store depletion in cells with and without σ1R ($n = 87$). (F and G) TIRF images of HeLa cells expressing Orai1-EGFP and σ1R-mKate either with (F) or without HA-STIM1 (G). Bars (C, D, F, and G), 10 μm. (H) Confocal images of HeLa cells expressing σ1R-EGFP, HA-STIM1, and Orai1-Myc, immunostained after treatment with 5 μM thapsigargin. Boxed areas in the left panels (bar, 5 μm) are enlarged on the right (bar, 2 μm). Arrowheads show colocalization of all three proteins as white puncta at the PM. (I) Summary results ($n = 8$) show Mander's overlap coefficient for colocalization of the indicated pairs of proteins in cells expressing only those tagged proteins or with σ1R-EGFP or HA-STIM1, as indicated, with and without thapsigargin treatment. **, $P < 0.01$; ***, $P < 0.001$, relative to resting cells. Student's t test. Results show mean ± SEM.
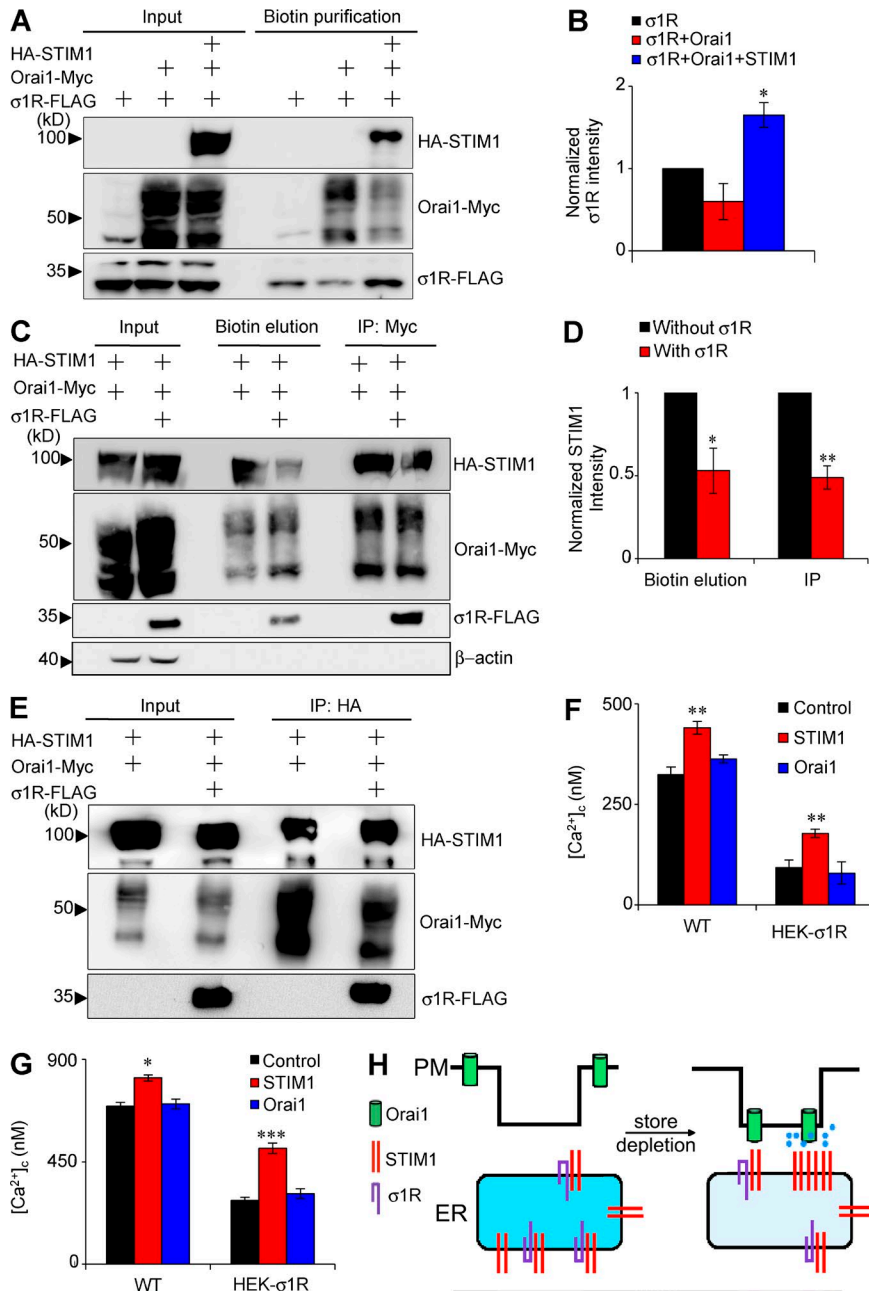
Figure 6. **STIM1, Orai1, and σ1R interact within a macromolecular complex at the PM.** (A) HEK cells expressing σ1R-FLAG alone or with Orai1-Myc or Orai1-Myc and HA-STIM1 were treated with thapsigargin (5 µM for 30 min in Ca²⁺-free HBS), and then the cell surface was biotinylated. The representative immunoblot shows the inputs and the proteins detected after purification with avidin beads. Input lanes were loaded with 10 µl of the 500-µl sample, and surface biotinylation lanes were loaded with 10 µl of the 50-µl eluate. (B) Summary shows the amounts of σ1R-FLAG detected in the avidin pull-downs (normalized to cells expressing only σ1R-FLAG). (C) HEK cells expressing Orai1-Myc and HA-STIM1 with or without σ1R-FLAG were cell surface biotinylated before sequential purification by elution from avidin-agarose with biotin and then from anti-Myc–agarose with Myc peptide. The immunoblot (anti-HA, anti-FLAG, anti-Myc, and anti–β-actin) shows the input and the two eluates. Input lanes were loaded with 10 µl of the 500-µl sample and elution lanes with 10 µl of the 50-µl eluate. (D) Summary shows the amounts of HA-STIM1 detected in the avidin (biotin elution) and anti-Myc pull-downs (normalized to Orai1-Myc pull-down in each condition). (E) HEK cells expressing Orai1-Myc and HA-STIM1 with or without σ1R-FLAG were immunoprecipitated (IP) with anti-HA antibody. (F) Peak [Ca²⁺]$_c$ signals evoked by SOCE were recorded from HEK or HEK-σ1R cells after treatment with thapsigargin (5 µM in Ca²⁺-free HBS for 10 min) and then restoration of 4 mM extracellular Ca²⁺. The effects of transiently overexpressing STIM1 or Orai1 are shown. WT, wild type. (G) The Ca²⁺ contents of the intracellular stores of the same cells were measured by recording peak increases in [Ca²⁺]$_c$ from cells exposed to ionomycin (5 µM in Ca²⁺-free HBS). Results (B, D, F, and G) are mean ± SEM. n = 3. *, $P < 0.05$; **, $P < 0.01$; ***, $P < 0.001$, relative to control. ANOVA with Tukey's posthoc analysis (B, F, and G) and Student's t test (D). (H) The results suggest that STIM1 and σ1R within the ER are associated. When STIM1 is activated by depletion of the ER Ca²⁺ stores, STIM1 conveys σ1R to the PM, where STIM1 and Orai1 associate, trapping them within ER–PM junctions. The interaction between STIM1 and Orai1 is weakened by σ1R.

the amount of Orai1 that copurified with STIM1 was reduced in the presence of σ1R (Fig. 6 E).

If the reduction in STIM1 binding to Orai1 contributes to inhibition of SOCE by σ1R, we might expect increased expression of STIM1 to relieve the inhibition. We therefore tested the effects of overexpressing STIM1 on the amplitude of SOCE in wild-type HEK and HEK-σ1R cells. Expression of STIM1 produced a similar increase in the amplitude of SOCE in wild-type and HEK-σ1R cells, but the percent increase was greater in the HEK-σ1R cells (36 ± 5% in wild-type and 81 ± 8% in HEK-σ1R cells; Fig. 6 F). This suggests that activation of SOCE is more limited by STIM1 in HEK-σ1R cells than in wild-type cells. The effects of STIM1 on SOCE were matched by its effects on Ca²⁺ stores: overexpression of STIM1 increased the Ca²⁺ content of the stores, and the effect was greater in HEK-σ1R relative to wild-type cells (83 ± 7% and 18 ± 5% increases, respectively; Fig. 6 G). Furthermore, the effects of

σ1R ligands on SOCE were much reduced in HEK-σ1R cells overexpressing STIM1 and Orai1 (Fig. S5). These results support the idea that σ1Rs inhibit the association of STIM1 with PM Orai1, thereby reducing SOCE (Fig. 6 H). Coincident with this inhibition of SOCE by σ1Rs, we invariably detected a decrease in the Ca²⁺ content of the ER.

σ1R inhibits binding of STIM1 to PM Orai1 channel complexes

To examine the structure of the PM Orai1 channel complex in the presence and absence of σ1R, we used atomic force microscopy (AFM). Previous AFM images of complexes purified from cells overexpressing Orai1 and STIM1 showed a hexameric arrangement of STIM1 around a central Orai1 complex and a few strings of STIM1 molecules associated with Orai1, consistent with the oligomerization of STIM1 after depletion of Ca²⁺ stores (Balasuriya et al., 2014b). We examined extracts from
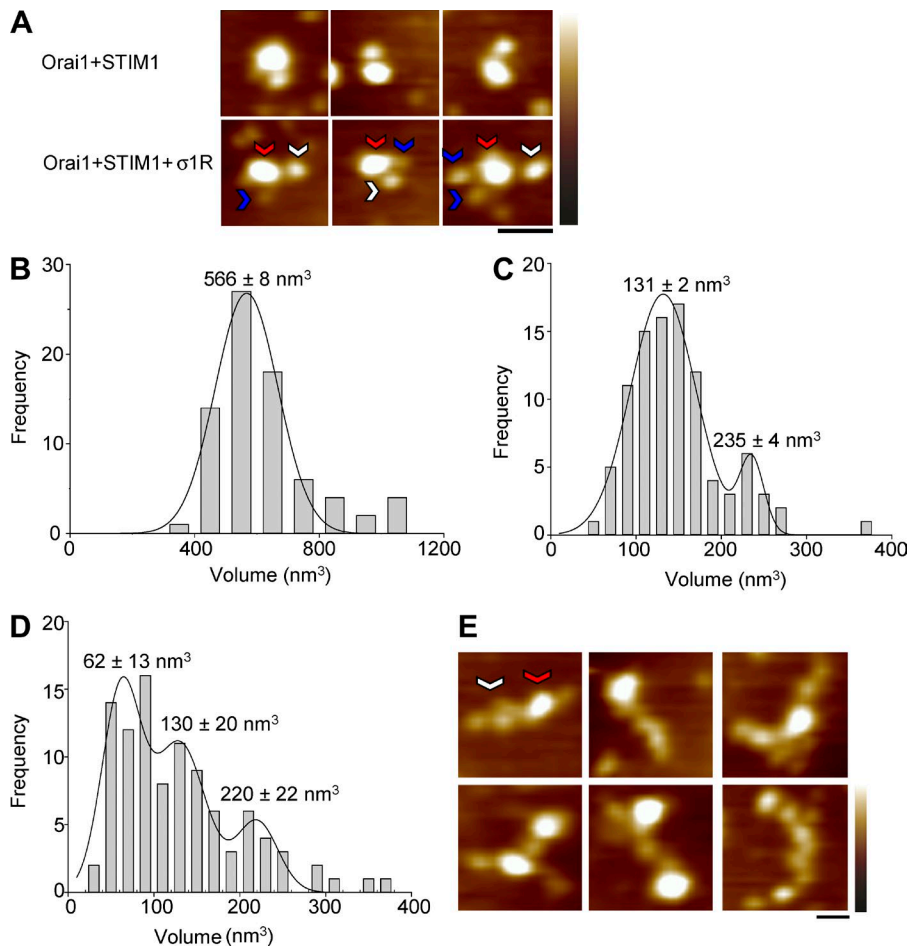
Figure 7. **AFM analyses of interactions between σ1R, STIM1, and Orai1 at the PM.** (A) AFM images of Orai1 isolated with σ1R and STIM1 showing the central Orai1 (red arrowheads) channel decorated by either STIM1 (white arrowheads) or both STIM1 and σ1R (blue arrowheads). (B–D) Frequency distributions of the volumes of the decorated central particles (Orai1; B), bound peripheral particles (STIM1) from cells expressing Orai1 and STIM1 (C), and bound peripheral particles (σ1R and STIM1) from cells expressing Orai1, STIM1, and σ1R (D). For these analyses, volume ranges of 30–100 nm^3 and 120–300 nm^3 were set for σ1R and STIM1 particles, respectively; the intermediate volumes (100–120 nm^3) were disregarded. (E) AFM images showing strings of STIM1 (white arrowhead) connecting several Orai1 channels (red arrowhead). These infrequent structures were observed only in the absence of σ1Rs. Bars, 20 nm; height scales, 0–3 nm (dark to light).

thapsigargin-treated HEK cells expressing Orai1-Myc/His and HA-STIM1, with or without σ1R-FLAG, in which cell surface proteins had been biotinylated and complexes were isolated by sequential purification using avidin and anti-Myc beads. AFM images showed large particles decorated by smaller peripheral particles (Fig. 7 A). The large central particle had the volume expected of hexameric Orai1 (566 ± 8 nm^3; Fig. 7 B). A volume distribution of bound peripheral particles for the Orai1-Myc/HA-STIM1 sample had two peaks at 131 ± 2 and 235 ± 4 nm^3 (Fig. 7 C), consistent with the expected volumes of STIM1 monomers and dimers. For the Orai1-Myc/HA-STIM1/σ1R-FLAG sample, the volume distribution of the peripheral particles had three peaks (62 ± 13, 130 ± 20, and 220 ± 22 nm^3) corresponding to STIM1 monomers and dimers and a smaller peak consistent with the expected volume of σ1R monomers (∼63 nm^3; Fig. 7 D). Of the 300 Orai1 complexes analyzed when expressed with STIM1 alone, 73 had bound particles and were either singly or doubly decorated. The total number of bound STIM1 was 96. From the 300 Orai1 complexes analyzed when coexpressed with STIM1 and σ1R, 76 had bound particles; there were 59 bound STIM1 and 46 bound σ1R. So the total number of bound STIM1 was reduced by 39% in the presence of σ1R. AFM images of Orai1 isolated from cells expressing Orai1 and STIM1 revealed, albeit with low frequency, that Orai1 bound to strings of STIM1 (Fig. 7 E). These assemblies were never seen in images from cells coexpressing σ1R. These results provide evidence for a PM complex of Orai1, STIM1, and σ1R and for reduced binding of STIM1 to Orai1 in the presence of σ1R.

σ1R inhibits SOCE via STIM1 rather than by direct effects on Orai1

Reduced binding of STIM1 to Orai1 caused by σ1R is expected to reduce SOCE, but σ1R might also directly inhibit gating of Orai1 channels. To address this possibility, we used the channel-activating domain (CAD) of STIM1, which directly activates Orai1 (Muik et al., 2009; Park et al., 2009; Yuan et al., 2009; Gudlur et al., 2014). mCh-CAD expressed alone in HeLa cells was diffusely distributed in the cytoplasm, but it was peripherally distributed when coexpressed with Orai1, consistent with the constitutive association of CAD and Orai1 (Fig. 8 A). Addition of extracellular Ca^{2+} to HEK or HEK-σ1R cells in Ca^{2+}-free HBS had no significant effect on $[Ca^{2+}]_c$, but there was a substantial increase in $[Ca^{2+}]_c$ in cells expressing CAD, consistent with constitutive activation of SOCE by CAD (Fig. 8, B and C). The response was indistinguishable in HEK and HEK-σ1R cells, suggesting that σ1R does not directly modulate PM expression of Orai1 nor its activity.

Discussion

We have shown that σ1Rs inhibit SOCE by decreasing the effectiveness with which empty stores stimulate Orai1. The target for regulation of SOCE by σ1R appears to be STIM1 (Fig. 8 D). σ1R and STIM1 colocalize in the ER; they can be coimmunoprecipitated before and after depletion of Ca^{2+} stores, and their interaction is regulated by σ1R ligands. The agonist, (+) SKF10047, increases binding of STIM1 to σ1R and further
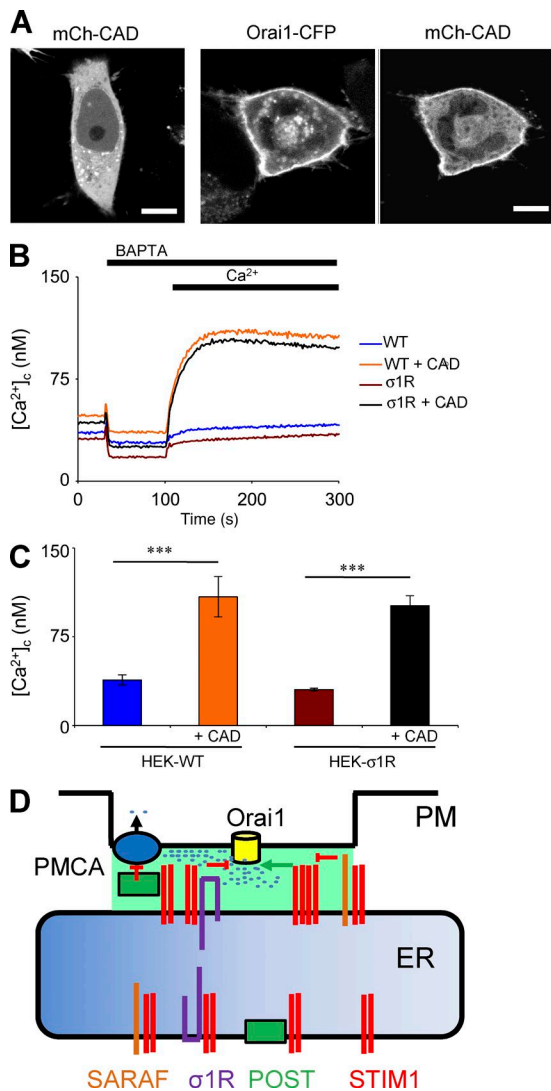
Figure 8. **Translocation of Ca^{2+}-regulating proteins to ER–PM junctions by STIM1.** (A) Confocal images of unstimulated HeLa cells transiently transfected with mCh-CAD alone (left) or with Orai1-CFP (right). Bars, 10 µm. (B) HEK or HEK-σ1R cells were mock transfected or transfected with CAD, and [Ca^{2+}]$_c$ was recorded after addition of 1 mM BAPTA and then restoration of 4 mM extracellular Ca^{2+}. WT, wild type. (C) Summary results show peak [Ca^{2+}]$_c$ signals evoked by restoration of extracellular Ca^{2+} (mean ± SD from six replicates). ***, P < 0.001, relative to control. Student's *t* test. (D) Several proteins, including POST, σ1R, and SARAF, associate with STIM1 in ER membranes (Krapivinsky et al., 2011; Palty et al., 2012). Loss of Ca^{2+} from the ER causes STIM1 molecules to oligomerize and become trapped, with their cargoes, in ER–PM junctions (green shading) as STIM1 binds to phosphatidylinositol 4,5-bisphosphate and Orai1. STIM1 activates Orai1 and thereby SOCE. The proteins associated with STIM1 also regulate SOCE. SARAF, by competing with STIM1, reduces STIM1 oligomerization and thereby contributes to the termination of SOCE (Palty et al., 2012). σ1R competes with STIM1 for binding to Orai1, thereby inhibiting SOCE. POST associates with and inhibits the PM Ca^{2+} pump (PMCA) and thereby reduces local Ca^{2+} extrusion (Krapivinsky et al., 2011).

inhibits SOCE, whereas the antagonist, BD1047, has the opposite effects. After store depletion, σ1R translocates with STIM1 to ER–PM junctions, but σ1R slows recruitment of STIM1 and reduces the amount of STIM1 bound to PM Orai1. This reduction in STIM1 binding to Orai1 suggests a likely mechanism for the inhibition of SOCE wherein σ1R accompanies STIM1 to ER–PM junctions, where it attenuates the interaction of STIM1

with Orai1. The gap between the ER and PM at the junctions where SOCE occurs is probably too large (>9 nm; Várnai et al., 2007) to be bridged by the short cytosolic loop of σ1R (Fig. S1; Hayashi and Su, 2007). The association of σ1Rs with PM Orai1 is therefore likely to be mediated by STIM1. Reduced binding of STIM1 to Orai1 in the presence of σ1R may be caused by σ1R inhibiting the oligomerization of STIM1 or directly reducing the affinity of STIM1 for Orai1.

There are interesting similarities between the behavior of σ1Rs and that of other ER membrane proteins, including SAR AF (Palty et al., 2012) and POST (partner of STIM1; Krapivinsky et al., 2011). SARAF also translocates to ER–PM junctions in a STIM1-dependent manner, and it promotes deactivation of STIM1 by antagonizing interactions between STIM1 molecules (Palty et al., 2012). Translocation of POST modulates SOCE-evoked Ca^{2+} signals because it inhibits the PM Ca^{2+} pump that extrudes cytosolic Ca^{2+} (Krapivinsky et al., 2011). Hence, after loss of Ca^{2+} from the ER, STIM1 both activates SOCE and fine-tunes its activity by delivering additional Ca^{2+}-regulating proteins to ER–PM junctions (Fig. 8 D). For σ1Rs, the effects of ER luminal Ca^{2+} on these delivery mechanisms may operate at two levels. Loss of ER Ca^{2+} (or a σ1R agonist) releases σ1R from its interaction with the ER luminal protein, BiP (Fig. S1; Hayashi and Su, 2007). Store depletion also causes STIM1 to oligomerize and thereby gain affinity for ER–PM junctions. Depletion of Ca^{2+} stores may therefore both release σ1R from its ER tethers and, via its association with oligomeric STIM1, allow it to accumulate at ER–PM junctions. We focused on SOCE, but recruitment of σ1Rs to ER–PM junctions by STIM1 might also be involved in regulation of other PM channels by σ1Rs (Maurice and Su, 2009; Su et al., 2010; Kourrich et al., 2013; Pabba, 2013). For example, the L-type Ca^{2+} channel is inhibited by σ1R (Tchedre et al., 2008) and by depletion of intracellular Ca^{2+} stores and STIM1 (Park et al., 2010; Wang et al., 2010). We suggest that STIM1-mediated translocation of σ1R to ER–PM junctions may inhibit voltage-gated Ca^{2+} entry and may also deliver σ1Rs to additional PM targets (Fig. 8 D).

Inhibition of SOCE by σ1Rs was invariably accompanied by a decrease in the Ca^{2+} content of the ER with no evident change in [Ca^{2+}]$_c$. In contrast, and consistent with a study by López et al. (2012), inhibition of SOCE by expression of Orai1^{E106Q} did not consistently affect ER Ca^{2+} content: it was normal in HEK cells but reduced in CHO cells. Inhibition of the STIM1–Orai1 interactions that mediate thapsigargin-evoked SOCE are not, therefore, sufficient to explain the effects of σ1Rs on ER Ca^{2+} content. It may be that σ1Rs also interact with STIM2, which plays a major role in maintaining the Ca^{2+} content of the stores (Brandman et al., 2007), or with other proteins, such as the sarco/ER Ca^{2+} ATPase, as was shown for orosomucoid-like 3 (Cantero-Recasens et al., 2010), or with Ca^{2+} channels that mediate Ca^{2+} uptake and release from the ER. For example, Sec61 mediates Ca^{2+} release from the ER, and it is inhibited by BiP (Schäuble et al., 2012). Expression of σ1R might sequester BiP (Fig. S1) and thereby enhance the Sec61-mediated Ca^{2+} leak. The decreased Ca^{2+} content of the ER might also arise from σ1R stabilizing IP$_3$R3 and thereby enhancing Ca^{2+} transport from the ER to mitochondria (Hayashi and Su, 2007).

The pathophysiological effects σ1Rs may, in part, result from inhibition of SOCE and the reduced Ca^{2+} content of the ER. The latter may affect protein folding (Hayashi and Su, 2007) and inhibit apoptosis by preventing excessive Ca^{2+} transfer to mitochondria (Maurice and Su, 2009; Giorgi et al., 2012).

The effects of σ1Rs on mitochondrial Ca^{2+} uptake are probably finely balanced because σ1Rs enhance delivery of Ca^{2+} to mitochondria at MAMs by stabilizing MAM-associated IP_3Rs (Hayashi and Su, 2007), whereas our results show that σ1Rs reduce the ER Ca^{2+} content. The latter could explain the otherwise surprising antiapoptotic effects of σ1Rs (Wang et al., 2005; Maurice and Su, 2009; Decuypere et al., 2011; Crottès et al., 2013). The σ1R agonist, cocaine, was recently shown to attenuate SOCE in rat brain microvascular endothelial cells (Brailoiu et al., 2016). The neuroprotective effects of σ1R agonists after ischemic injury (Katnik et al., 2006) and in patients with amyotrophic lateral sclerosis arising from loss-of-function mutations in σ1R (Al-Saif et al., 2011; Ono et al., 2014) may also, at least in part, be due to inhibition of SOCE. Hyperactive SOCE may contribute to the motor deficiencies in σ1R-knockout mice (Maurice and Su, 2009; Sabino et al., 2009; Mavlyutov et al., 2010) and to neurodegeneration in Alzheimer's (Mishina et al., 2008; Ishikawa and Hashimoto, 2009; Hyrskyluoto et al., 2013) and Parkinson's diseases (Mishina et al., 2005; Hyrskyluoto et al., 2013; Francardo et al., 2014), where expression of σ1R is reduced. These suggestions prompt consideration of whether σ1R also interacts with STIM2 because it appears to play the major role in regulating SOCE in central neurons (Berna-Erro et al., 2009).

We conclude that σ1Rs inhibit SOCE because they associate with STIM1, slow STIM1 recruitment to ER–PM junctions, and reduce its binding to Orai1 after depletion of Ca^{2+} stores. Our study highlights a role for STIM1 in translocating σ1Rs to the PM and establishes σ1Rs and their ligands as important regulators of SOCE, a ubiquitously expressed Ca^{2+} entry pathway (Fig. 8 D).

Materials and methods

Materials
(+)SKF10047 and BD1047 were from Tocris Bioscience. Ionomycin was from MerckEurolab. Thapsigargin was from Alomone Labs. Anti-Myc monoclonal antibody (1:500 dilution for immunoblots; 46–0603), fura 2–AM, and fluo 4–AM were from Thermo Fisher Scientific. Anti-HA (1:500; 16B12) and anti-FLAG (1:500; F3165) monoclonal antibodies were from Covance and Sigma-Aldrich, respectively. The anti-σ1R antibody (1:200; Ab53852), which recognizes a sequence conserved in human and mouse σ1R, was from Abcam. Custom-made rabbit polyclonal antipeptide antisera to STIM1 (1:100; CDPQHGH GSQRDLTR; the Cys used for conjugation is underlined) and Orai1 (1:200; CEFAWLQDQLDHRGD) were prepared by Sigma-Aldrich. Anti-actin (1:500; A5441) antibody was from Sigma-Aldrich. Anti–mouse (1:1,000) and anti–rabbit (1:1,000) HRP-conjugated secondary antibodies were from Thermo Fisher Scientific and Bio-Rad Laboratories, respectively. Sources of additional materials are provided within the relevant methods.

Plasmids and siRNA
Plasmids encoding HA-STIM1 and Orai1-Myc/His_6 have been described previously (Willoughby et al., 2012; Balasuriya et al., 2014b). For mCh-STIM1, human STIM1 was subcloned into mCherry-C1 (Takara Bio Inc.) using XbaI and NotI. For σ1R-FLAG, σ1R was subcloned into pcDNA3.1/FLAG using HindIII and AgeI. For σ1R-GFP, σ1R was subcloned into GFP-N1 (Takara Bio Inc.) using HindIII and KpnI. For σ1R-V5, σ1R was subcloned into pcDNA3.1/V5-His-TOPO using HindIII and AgeI. For σ1R-mKate, σ1R was subcloned into

mKate2-N (Evrogen) using HindIII and KpnI. The coding sequences of all new constructs were verified. pDsRed2-Mito was from Takara Bio Inc. A pSIREN vector encoding siRNA for σ1R (5′-GATCCA CACGTGGATGGTGGAGTATTCAAGAGATACTCCACCATCCAC GTGTTTTTTTGCTAGCG-3′) was used to inhibit expression of σ1R. pSIREN encoding the luciferase gene was used as a negative control. Both pSIREN constructs were gifts from T.-P. Su (National Institutes of Health, Bethesda, MD; Hayashi and Su, 2004). An expression plasmid (MO70) encoding a dominant-negative form of Orai1 in which Glu-106 is replaced by Gln (Orai1[E106Q]) was a gift from Y. Gwack and S. Srikanth (University of California, Los Angeles, Los Angeles, CA; Srikanth et al., 2012). The expression plasmid for mouse GFP-NFAT1 was a gift from A. Parekh (University of Oxford, Oxford, England, UK; Kar et al., 2011). The mCh-STIM1 CAD expression plasmid was a gift from P. Hogan (La Jolla Institute for Allergy and Immunology, La Jolla, CA; Gudlur et al., 2014), and Orai1-CFP was from D.M.F. Cooper (University of Cambridge, Cambridge, England, UK).

Cell culture and transfection
All cells were maintained in DMEM with 10% fetal bovine serum and 1% penicillin/streptomycin (Sigma-Aldrich) at 37°C in humidified air with 5% CO_2. tsA 201 cells were grown to 70% confluence in a 162-cm^2 flask and transfected using calcium phosphate. 50 µg of plasmid DNA was mixed with 5 ml of 250 mM $CaCl_2$ and diluted with 5 ml of medium comprising 275 mM NaCl, 10 mM KCl, 1.4 mM Na_2HPO_4, 15 mM glucose, and 42 mM Hepes, pH 7.07. The mixture was added to the cells bathed in 25 ml of fresh growth medium. After 8 h, the medium was replaced with fresh growth medium. Cells were incubated for a further 48 h before being used for experiments.

HEK 293 cells were transfected using polyethylenimine. For cells grown to 70% confluence in 1 well of a 6-well plate, 1 µg of plasmid DNA was mixed with 2 µl of 7.5 mM polyethylenimine (Polysciences, Inc.) and then diluted with 150 µl of serum-free DMEM. The mixture was incubated for 10 min at 20°C and then added to wells containing 2 ml of fresh growth medium for 48 h. The generation of a polyclonal HEK cell line stably expressing mouse σ1R-V5 (HEK-σ1R cells) was performed as described previously (Xu et al., 2012). These cells were maintained in medium supplemented with 0.8 mg/ml G418 (Thermo Fisher Scientific).

HeLa cells were grown on poly-L-lysine–coated 25-mm glass coverslips and transfected using Lipofectamine 2000 (Thermo Fisher Scientific). For 1 well of a 6-well plate, 2 µg of plasmid DNA was diluted in 200 µl Opti-MEM and incubated at 20°C for 5 min. This was combined with 200 µl Opti-MEM containing 4 µl Lipofectamine 2000 and left for a further 20 min at 20°C. The mixture was then added to cells in 2 ml of fresh medium. Cells were incubated for 48 h at 37°C and then used for experiments.

Measurements of $[Ca^{2+}]_c$
For measurements of $[Ca^{2+}]_c$ in populations of cells, HEK cells were seeded into poly-L-lysine–coated 96-well plates. After 24 h, cells were incubated with 2 µM fluo 4–AM in HBS for 60 min at 20°C. HBS had the following composition: 150 mM NaCl, 10 mM KCl, 1 mM $MgCl_2$, 2 mM $CaCl_2$, 10 mM glucose, and 10 mM Hepes, pH 7.3. In Ca^{2+}-free HBS, Ca^{2+} was omitted, and 1 mM BAPTA was added. For treatments with (+)SKF10047 and BD1047, 10 mM stock solutions were prepared in DMSO and water, respectively. Cells were pretreated with 25 µM (+)SKF10047 or 10 µM BD1047 in serum-free DMEM for 1 h at 37°C before loading cells with fluorescent Ca^{2+} indicators. Drug treatments were continued during loading and throughout $[Ca^{2+}]_c$ measurements. After loading, cells were washed and incubated in HBS for a further 30 min at 20°C. Fluorescence (excitation at 490 nm and emission at

520 nm) was measured at 20°C using a plate reader that allows on-line additions (FlexStation 3; Molecular Devices). Fluorescence was calibrated to $[Ca^{2+}]_c$ from

$$[Ca^{2+}]_c = K_D\left(\frac{F - F_{min}}{F_{max} - F}\right),$$

where $K_D = 345$ nM ($K_D = 190$ nM at 37°C; Fig. S2 B), F is the measured fluorescence, and F_{max} and F_{min} are the fluorescence values determined after addition of 0.1% Triton X-100 in HBS with 10 mM Ca^{2+} or 10 mM BAPTA, respectively.

Measurements of Mn^{2+} entry
Confluent cultures of HEK cells in 96-well plates were loaded with 2 µM fura 2–AM using the method described for fluo 4. Fluorescence (excitation at 360 nm and emission at 510 nm) was measured using a plate reader (FlexStation 3) at 1.5-s intervals at 20°C. Quenching of fura 2 fluorescence (which reports unidirectional entry of Mn^{2+}) is reported as F/F_0, where F is the fluorescence intensity recorded at each time and F_0 is the mean fluorescence intensity measured in the 5 s before addition of $MnCl_2$. Monoexponential curve fits to the time course of the changes in F/F_0 were used to compute half-times ($t_{1/2}$) for Mn^{2+}-evoked fluorescence quenching.

NFAT translocation assay
HEK cells were seeded onto poly-L-lysine–coated 25-mm coverslips, transfected with GFP-NFAT plasmid using polyethylenimine, and used after 48 h. The distribution of GFP fluorescence was measured before and 40 min after addition of 5 µM thapsigargin to cells at 37°C in HBS. Fluorescence (excitation at 488 nm and emission at 510–540 nm) was collected using a confocal microscope (SP5; Leica Biosystems) with an oil-immersion 40× objective (NA 1.25). Analyses of nuclear translocation of GFP-NFAT were performed with coded images, which were decoded only when the analysis was complete.

Analyses of protein expression
Cells were grown in 162-cm² flasks. Where appropriate, cells were transfected with 50 µg of plasmid DNA using polyethylenimine. Cells were extracted in ice-cold medium (138 mM NaCl, 5 mM KCl, 1 mM Na_2HPO_4, 7.5 mM glucose, 21 mM Hepes, and 2 mM EDTA, pH 7.4) and centrifuged at 1,000 g for 5 min. Pelleted cells were solubilized at 4°C for 60 min in Triton solution (TS) containing 25 mM Tris-HCl, 150 mM NaCl, 10 mM EDTA, 1% Triton X-100, and 1 mg/ml protease inhibitor cocktail solution (Roche), pH 7.4, and samples were analyzed by SDS-PAGE followed by immunoblotting.

Immunoprecipitation analyses
tsA 201 cells, which are SV40-transformed HEK 293 cells, were used because they express heterologous proteins at high levels. Cells were grown in 162-cm² flasks and transfected using calcium phosphate. Pretreatments with (+)SKF10047 and BD1047 were for 2 h at 37°C, and stimulation with 5 µM thapsigargin was for 30 min at 20°C. Cells were extracted in 25 ml of ice-cold medium, and all subsequent steps were performed at 4°C. The suspension was centrifuged at 1,000 g for 5 min, and pelleted cells were solubilized for 60 min in 500 µl TS. After centrifugation (50,000 g for 60 min), 50 µl of the supernatant was removed for analysis of total expression (input), and 450 µl was incubated with 30 µl anti-Myc (EZ View Red) or anti-FLAG beads (Sigma-Aldrich) for 3 h with rotation. Protein–bead complexes were isolated (20,800 g for 10 min) and washed three times in TS, and proteins were eluted either with 50 µl of the peptides (1 mg/ml; Sigma-Aldrich), to which the anti-Myc or anti-FLAG antibodies had been raised, or with 50 µl Laemmli buffer. The eluted samples were analyzed by SDS-PAGE followed by immunoblotting.

For immunoblots, lanes were loaded with 10 µl of the 500-µl sample (2% of the entire sample) for the measurement of input and with 10 or 20 µl of the 50-µl eluate for measurements of immunoprecipitation.

Isolation of surface biotinylated proteins
tsA 201 cells were grown in 162-cm² flasks and transfected using calcium phosphate. After appropriate stimulation, the medium was removed and replaced with 12.5 ml of ice-cold HBS containing 0.2 mg/ml biotin-sulfo-NHS (Thermo Fisher Scientific). After 60 min on ice, cells were washed three times with 15 ml Tris-buffered saline (25 mM Tris-HCl, 150 mM NaCl, and 10 mM EDTA, pH 7.4) and centrifuged at 1,000 g for 5 min, and the pellet was solubilized in 500 µl TS for 60 min at 4°C. After centrifugation at 50,000 g for 60 min, the supernatant was incubated with 50 µl monomeric avidin-coated agarose beads (Thermo Fisher Scientific) at 4°C for 2 h. Protein–bead complexes were collected at 20,800 g for 10 min, washed three times in TS, and eluted with either 50 µl Laemmli buffer for immunoblots or biotin (1 mg/ml in 1 ml TS) for further immunopurification using anti-Myc beads as described in the previous paragraph. For analyses of avidin pull-downs of biotinylated proteins (Fig. 5, C–E), 2% of the total sample was loaded as input, and 40% of the Laemmli sample was loaded in the surface biotinylation lanes.

Immunostaining
HeLa cells were seeded on poly-L-lysine–coated glass coverslips, transfected, and used after 48 h. After stimulation, cells were washed with ice-cold PBS (137 mM NaCl, 2.7 mM KCl, 10 mM Na_2HPO_4, and 2 mM KH_2PO_4), fixed with 4% paraformaldehyde for 20 min, and permeabilized with 0.5 mg/ml saponin for 60 min (Sigma-Aldrich) in blocking solution (5% goat serum and 3% BSA in PBS). Cells were stained with primary antibody in blocking solution (PBS containing 3% BSA and 5% goat serum) for 60 min at 20°C, washed twice with PBS, and then incubated in the dark with secondary antibody in blocking solution for 60 min at 20°C, washed with PBS, dried, mounted onto a glass microscope slide, and stored at 4°C. Cells were imaged using an oil-immersion 60× objective (NA 1.40) using a confocal microscope (SP5; Leica Biosystems). For both Pearson's and Mander's coefficient measurements, images were analyzed with ImageJ (National Institutes of Health) using the JACoP plugin. For Mander's coefficient, only pixels in which HA-STIM1 (or σ1R-EGFP) was detected were considered, and the fraction of those pixels in which Orai1-Myc was also detected was then computed to provide the colocalization coefficient.

TIRF microscopy
Coverslips were mounted on a TIRF microscope (IX51 inverted microscope [Olympus] with a 100× oil-immersion objective [NA 1.49] coupled to an electron-multiplying charged-coupled device camera [iXon; Andor Technology] and 488-nm argon ion and 561-nm diode lasers). Cells were incubated with HBS at 20°C and imaged (1 image/s) by exciting σ1R-GFP at 488 nm (emission at 510–540 nm) and mCh-STIM1 at 561 nm (emission at 610–650 nm). For each experiment, there were suitable controls, with cells expressing the EGFP-tagged protein alone and the mCherry/mKate-tagged protein alone to ensure there was no bleed through. For depletion of stores, cells were incubated with 1 µM thapsigargin in Ca^{2+}-free HBS. Fluorescence intensities were quantified using the time series analyzer plugin V2.0 in ImageJ. Individual regions of interest within the cell were selected, and the data were analyzed as F/F_0, where F and F_0 are the fluorescence intensities at each time and at the start of the experiment, respectively.

AFM
tsA 201 cells expressing appropriate combinations of Orai1-Myc-His, σ1R-FLAG, and HA-STIM1 were treated with thapsigargin, followed

by biotin-sulfo-NHS, and then purified using sequential avidin and anti-Myc affinity chromatography, as described in the Isolation of surface biotinylated proteins section. About 45 µl of proteins was added to a 1-cm² mica disk, incubated at 20°C for 10 min, gently washed with water, and dried under nitrogen. Samples were imaged in air using an atomic force microscope (Multimode; Bruker). The silicon cantilever (OTESPA; Bruker) was set at a drive frequency of 271–321 kHz and spring constant of 12–103 N/m. The scan rate was 3 Hz, and the applied imaging force was kept as low as possible (target amplitude of 1.0 V and amplitude set point of 0.7–1.0 V). Molecular volumes for individual particles were determined using an image processor (version 5; Scanning Probe). For particles within complexes, particle heights (h) and radii (r) were measured manually using Nanoscope software. Particle volumes (V_m) were then calculated from

$$V_m = \frac{\pi h (3\,r^2 + h^2)}{6}.$$

Molecular volume (V_c), based on a known molecular mass (M_0), was calculated from

$$V_c = \frac{M_0(V_1 + dV_2)}{N_0},$$

where N_0 is Avogadro's number, V_1 is the specific particle volume (0.74 cm³/g), V_2 is the water specific volume (1 cm³/g), and d is the extent of hydration (assumed to be 0.4 g H_2O/g protein).

Data analysis

Most results are presented as mean ± SEM from n independent experiments. Statistical analysis used Student's t test or analysis of variance (ANOVA) followed by Tukey's posthoc test as appropriate.

Online supplemental material

Fig. S1 illustrates key features of σ1R, and Table S1 describes ligands targeting σ1R. Fig. S2 shows the effects of expressing σ1Rs in HEK cells on SOCE and the Ca^{2+} content of the intracellular stores. Fig. S3 shows the effects of σ1R ligands on SOCE in CHO and HEK cells. Fig. S4 shows the effects of σ1R ligands on SOCE and the Ca^{2+} content of the intracellular stores in MDA-MB-231 human breast cancer cells. Fig. S5 shows the effects of σ1R ligands on SOCE in HEK-σ1R cells overexpressing STIM1 and Orai1. Online supplemental material is available at http://www.jcb.org/cgi/content/full/jcb.201506022/DC1.

References

Al-Saif, A., F. Al-Mohanna, and S. Bohlega. 2011. A mutation in sigma-1 receptor causes juvenile amyotrophic lateral sclerosis. *Ann. Neurol.* 70:913–919. http://dx.doi.org/10.1002/ana.22534

Aydar, E., C.P. Palmer, V.A. Klyachko, and M.B. Jackson. 2002. The sigma receptor as a ligand-regulated potassium channel subunit. *Neuron.* 34:399–410. http://dx.doi.org/10.1016/S0896-6273(02)00677-3

Aydar, E., P. Onganer, R. Perrett, M.B. Djamgoz, and C.P. Palmer. 2006. The expression and functional characterization of sigma (σ) 1 receptors in breast cancer cell lines. *Cancer Lett.* 242:245–257. http://dx.doi.org/10.1016/j.canlet.2005.11.011

Balasuriya, D., A.P. Stewart, D. Crottès, F. Borgese, O. Soriani, and J.M. Edwardson. 2012. The sigma-1 receptor binds to the Nav1.5 voltage-gated Na⁺ channel with 4-fold symmetry. *J. Biol. Chem.* 287:37021–37029. http://dx.doi.org/10.1074/jbc.M112.382077

Balasuriya, D., L. D'Sa, R. Talker, E. Dupuis, F. Maurin, P. Martin, F. Borgese, O. Soriani, and J.M. Edwardson. 2014a. A direct interaction between the sigma-1 receptor and the hERG voltage-gated K⁺ channel revealed by atomic force microscopy and homogeneous time-resolved fluorescence (HTRF®). *J. Biol. Chem.* 289:32353–32363. http://dx.doi.org/10.1074/jbc.M114.603506

Balasuriya, D., S. Srivats, R.D. Murrell-Lagnado, and J.M. Edwardson. 2014b. Atomic force microscopy (AFM) imaging suggests that stromal interaction molecule 1 (STIM1) binds to Orai1 with sixfold symmetry. *FEBS Lett.* 588:2874–2880. http://dx.doi.org/10.1016/j.febslet.2014.06.054

Berna-Erro, A., A. Braun, R. Kraft, C. Kleinschnitz, M.K. Schuhmann, D. Stegner, T. Wultsch, J. Eilers, S.G. Meuth, G. Stoll, and B. Nieswandt. 2009. STIM2 regulates capacitive Ca^{2+} entry in neurons and plays a key role in hypoxic neuronal cell death. *Sci. Signal.* 2:ra67. http://dx.doi.org/10.1126/scisignal.2000522

Brailoiu, G.C., E. Deliu, L.M. Console-Bram, J. Soboloff, M.E. Abood, E.M. Unterwald, and E. Brailoiu. 2016. Cocaine inhibits store-operated Ca2+ entry in brain microvascular endothelial cells: critical role for sigma-1 receptors. *Biochem. J.* 473:1–5. http://dx.doi.org/10.1042/BJ2015093426467159

Brandman, O., J. Liou, W.S. Park, and T. Meyer. 2007. STIM2 is a feedback regulator that stabilizes basal cytosolic and endoplasmic reticulum Ca^{2+} levels. *Cell.* 131:1327–1339. http://dx.doi.org/10.1016/j.cell.2007.11.039

Brune, S., S. Pricl, and B. Wünsch. 2013. Structure of the σ1 receptor and its ligand binding site. *J. Med. Chem.* 56:9809–9819. http://dx.doi.org/10.1021/jm400660u

Cantero-Recasens, G., C. Fandos, F. Rubio-Moscardo, M.A. Valverde, and R. Vicente. 2010. The asthma-associated ORMDL3 gene product regulates endoplasmic reticulum-mediated calcium signaling and cellular stress. *Hum. Mol. Genet.* 19:111–121. http://dx.doi.org/10.1093/hmg/ddp471

Cárdenas, C., R.A. Miller, I. Smith, T. Bui, J. Molgó, M. Müller, H. Vais, K.H. Cheung, J. Yang, I. Parker, et al. 2010. Essential regulation of cell bioenergetics by constitutive InsP₃ receptor Ca^{2+} transfer to mitochondria. *Cell.* 142:270–283. http://dx.doi.org/10.1016/j.cell.2010.06.007

Chu, U.B., and A.E. Ruoho. 2016. Biochemical pharmacology of the Sigma-1 receptor. *Mol. Pharmacol.* 89:142–153. http://dx.doi.org/10.1124/mol.115.101170

Cobos, E.J., J.M. Entrena, F.R. Nieto, C.M. Cendán, and E. Del Pozo. 2008. Pharmacology and therapeutic potential of sigma1 receptor ligands. *Curr. Neuropharmacol.* 6:344–366. http://dx.doi.org/10.2174/157015908787386113

Crottès, D., S. Martial, R. Rapetti-Mauss, D.F. Pisani, C. Loriol, B. Pellissier, P. Martin, E. Chevet, F. Borgese, and O. Soriani. 2011. Sig1R protein regulates hERG channel expression through a post-translational mechanism in leukemic cells. *J. Biol. Chem.* 286:27947–27958. http://dx.doi.org/10.1074/jbc.M111.226738

Crottès, D., H. Guizouarn, P. Martin, F. Borgese, and O. Soriani. 2013. The sigma-1 receptor: a regulator of cancer cell electrical plasticity? *Front. Physiol.* 4:175. http://dx.doi.org/10.3389/fphys.2013.00175

Decuypere, J.P., G. Monaco, G. Bultynck, L. Missiaen, H. De Smedt, and J.B. Parys. 2011. The IP₃ receptor-mitochondria connection in apoptosis and autophagy. *Biochim. Biophys. Acta.* 1813:1003–1013. http://dx.doi.org/10.1016/j.bbamcr.2010.11.023

DeHaven, W.I., B.F. Jones, J.G. Petranka, J.T. Smyth, T. Tomita, G.S. Bird, and J.W. Putney Jr. 2009. TRPC channels function independently of STIM1 and Orai1. *J. Physiol.* 587:2275–2298. http://dx.doi.org/10.1113/jphysiol.2009.170431

Francardo, V., F. Bez, T. Wieloch, H. Nissbrandt, K. Ruscher, and M.A. Cenci. 2014. Pharmacological stimulation of sigma-1 receptors has neurorestorative effects in experimental parkinsonism. *Brain.* 137:1998–2014. http://dx.doi.org/10.1093/brain/awu107

Giorgi, C., F. Baldassari, A. Bononi, M. Bonora, E. De Marchi, S. Marchi, S. Missiroli, S. Patergnani, A. Rimessi, J.M. Suski, et al. 2012. Mitochondrial Ca^{2+} and apoptosis. *Cell Calcium.* 52:36–43. http://dx.doi .org/10.1016/j.ceca.2012.02.008

Gromek, K.A., F.P. Suchy, H.R. Meddaugh, R.L. Wrobel, L.M. LaPointe, U.B. Chu, J.G. Primm, A.E. Ruoho, A. Senes, and B.G. Fox. 2014. The oligomeric states of the purified sigma-1 receptor are stabilized by ligands. *J. Biol. Chem.* 289:20333–20344. http://dx.doi.org/10.1074/jbc .M113.537993

Gudlur, A., A. Quintana, Y. Zhou, N. Hirve, S. Mahapatra, and P.G. Hogan. 2014. STIM1 triggers a gating rearrangement at the extracellular mouth of the ORAI1 channel. *Nat. Commun.* 5:5164. http://dx.doi.org/10.1038 /ncomms6164

Hayashi, T., and T.-P. Su. 2003. Intracellular dynamics of σ-1 receptors (σ$_1$ binding sites) in NG108-15 cells. *J. Pharmacol. Exp. Ther.* 306:726–733. http://dx.doi.org/10.1124/jpet.103.051292

Hayashi, T., and T.-P. Su. 2004. Sigma-1 receptors at galactosylceramide-enriched lipid microdomains regulate oligodendrocyte differentiation. *Proc. Natl. Acad. Sci. USA.* 101:14949–14954. http://dx.doi.org/10.1073 /pnas.0402890101

Hayashi, T., and T.-P. Su. 2005a. The sigma receptor: evolution of the concept in neuropsychopharmacology. *Curr. Neuropharmacol.* 3:267–280. http://dx .doi.org/10.2174/157015905774322516

Hayashi, T., and T.-P. Su. 2005b. The potential role of sigma-1 receptors in lipid transport and lipid raft reconstitution in the brain: implication for drug abuse. *Life Sci.* 77:1612–1624. http://dx.doi.org/10.1016/j.lfs.2005.05.009

Hayashi, T., and T.-P. Su. 2007. Sigma-1 receptor chaperones at the ER-mitochondrion interface regulate Ca^{2+} signaling and cell survival. *Cell.* 131:596–610. http://dx.doi.org/10.1016/j.cell.2007.08.036

Hogan, P.G., and A. Rao. 2015. Store-operated calcium entry: Mechanisms and modulation. *Biochem. Biophys. Res. Commun.* 460:40–49. http://dx.doi .org/10.1016/j.bbrc.2015.02.110

Hoth, M., and B.A. Niemeyer. 2013. The neglected CRAC proteins: Orai2, Orai3, and STIM2. *Curr. Top. Membr.* 71:237–271. http://dx.doi.org/10 .1016/B978-0-12-407870-3.00010-X

Hyrskyluoto, A., I. Pulli, K. Törnqvist, T.H. Ho, L. Korhonen, and D. Lindholm. 2013. Sigma-1 receptor agonist PRE084 is protective against mutant huntingtin-induced cell degeneration: involvement of calpastatin and the NF-κB pathway. *Cell Death Dis.* 4:e646. http://dx.doi.org/10.1038/cddis.2013.170

Ishikawa, M., and K. Hashimoto. 2009. The role of sigma-1 receptors in the pathophysiology of neuropsychiatric diseases. *J. Receptor Ligand Channel Res.* 2010:25–36. http://dx.doi.org/10.2147/JRLCR.S8453

Ito, K., Y. Hirooka, R. Matsukawa, M. Nakano, and K. Sunagawa. 2012. Decreased brain sigma-1 receptor contributes to the relationship between heart failure and depression. *Cardiovasc. Res.* 93:33–40. http://dx.doi.org /10.1093/cvr/cvr255

Ito, K., Y. Hirooka, and K. Sunagawa. 2013. Brain sigma-1 receptor stimulation improves mental disorder and cardiac function in mice with myocardial infarction. *J. Cardiovasc. Pharmacol.* 62:222–228. http://dx.doi.org/10 .1097/FJC.0b013e3182970b15

Kar, P., C. Nelson, and A.B. Parekh. 2011. Selective activation of the transcription factor NFAT1 by calcium microdomains near Ca^{2+} release-activated Ca^{2+} (CRAC) channels. *J. Biol. Chem.* 286:14795–14803. http://dx.doi.org/10 .1074/jbc.M111.220582

Katnik, C., W.R. Guerrero, K.R. Pennypacker, Y. Herrera, and J. Cuevas. 2006. Sigma-1 receptor activation prevents intracellular calcium dysregulation in cortical neurons during in vitro ischemia. *J. Pharmacol. Exp. Ther.* 319:1355–1365. http://dx.doi.org/10.1124/jpet.106.107557

Kilch, T., D. Alansary, M. Peglow, K. Dörr, G. Rychkov, H. Rieger, C. Peinelt, and B.A. Niemeyer. 2013. Mutations of the Ca^{2+}-sensing stromal interaction molecule STIM1 regulate Ca^{2+} influx by altered oligomerization of STIM1 and by destabilization of the Ca^{2+} channel Orai1. *J. Biol. Chem.* 288:1653–1664. http://dx.doi.org/10.1074/jbc.M112.417246

Kourrich, S., T. Hayashi, J.-Y. Chuang, S.-Y. Tsai, T.-P. Su, and A. Bonci. 2013. Dynamic interaction between sigma-1 receptor and Kv1.2 shapes neuronal and behavioral responses to cocaine. *Cell.* 152:236–247. http:// dx.doi.org/10.1016/j.cell.2012.12.004

Krapivinsky, G., L. Krapivinsky, S.C. Stotz, Y. Manasian, and D.E. Clapham. 2011. POST, partner of stromal interaction molecule 1 (STIM1), targets STIM1 to multiple transporters. *Proc. Natl. Acad. Sci. USA.* 108:19234–19239. http://dx.doi.org/10.1073/pnas.1117231108

Lewis, R.S. 2007. The molecular choreography of a store-operated calcium channel. *Nature.* 446:284–287. http://dx.doi.org/10.1038/nature05637

Lewis, A., T. Hayashi, T.-P. Su, and M.J. Betenbaugh. 2014. Bcl-2 family in inter-organelle modulation of calcium signaling; roles in bioenergetics and cell survival. *J. Bioenerg. Biomembr.* 46:1–15. http://dx.doi.org/10 .1007/s10863-013-9527-7

Liou, J., M. Fivaz, T. Inoue, and T. Meyer. 2007. Live-cell imaging reveals sequential oligomerization and local plasma membrane targeting of stromal interaction molecule 1 after Ca^{2+} store depletion. *Proc. Natl. Acad. Sci. USA.* 104:9301–9306. http://dx.doi.org/10.1073/pnas.0702866104

López, E., G.M. Salido, J.A. Rosado, and A. Berna-Erro. 2012. Unraveling STIM2 function. *J. Physiol. Biochem.* 68:619–633. http://dx.doi.org/10 .1007/s13105-012-0163-1

Lupardus, P.J., R.A. Wilke, E. Aydar, C.P. Palmer, Y. Chen, A.E. Ruoho, and M.B. Jackson. 2000. Membrane-delimited coupling between sigma receptors and K$^+$ channels in rat neurohypophysial terminals requires neither G-protein nor ATP. *J. Physiol.* 526:527–539. http://dx.doi.org/10 .1111/j.1469-7793.2000.00527.x

Mallilankaraman, K., P. Doonan, C. Cárdenas, H.C. Chandramoorthy, M. Müller, R. Miller, N.E. Hoffman, R.K. Gandhirajan, J. Molgó, M.J. Birnbaum, et al. 2012. MICU1 is an essential gatekeeper for MCU-mediated mitochondrial Ca^{2+} uptake that regulates cell survival. *Cell.* 151:630–644. http://dx.doi.org/10.1016/j.cell.2012.10.011

Maurice, T., and T.-P. Su. 2009. The pharmacology of sigma-1 receptors. *Pharmacol. Ther.* 124:195–206. http://dx.doi.org/10.1016/j.pharmthera .2009.07.001

Maurice, T., V.L. Phan, A. Urani, H. Kamei, Y. Noda, and T. Nabeshima. 1999. Neuroactive neurosteroids as endogenous effectors for the sigma$_1$ (σ$_1$) receptor: pharmacological evidence and therapeutic opportunities. *Jpn. J. Pharmacol.* 81:125–155. http://dx.doi.org/10.1254/jjp.81.125

Maurice, T., R. Martin-Fardon, P. Romieu, and R.R. Matsumoto. 2002. Sigma$_1$ (σ$_1$) receptor antagonists represent a new strategy against cocaine addiction and toxicity. *Neurosci. Biobehav. Rev.* 26:499–527. http://dx .doi.org/10.1016/S0149-7634(02)00017-9

Mavlyutov, T.A., M.L. Epstein, K.A. Andersen, L. Ziskind-Conhaim, and A.E. Ruoho. 2010. The sigma-1 receptor is enriched in postsynaptic sites of C-terminals in mouse motoneurons. An anatomical and behavioral study. *Neuroscience.* 167:247–255. http://dx.doi.org/10.1016 /j.neuroscience.2010.02.022

Miki, Y., F. Mori, T. Kon, K. Tanji, Y. Toyoshima, M. Yoshida, H. Sasaki, A. Kakita, H. Takahashi, and K. Wakabayashi. 2014. Accumulation of the sigma-1 receptor is common to neuronal nuclear inclusions in various neurodegenerative diseases. *Neuropathology.* 34:148–158. http://dx.doi .org/10.1111/neup.12080

Mishina, M., K. Ishiwata, K. Ishii, S. Kitamura, Y. Kimura, K. Kawamura, K. Oda, T. Sasaki, O. Sakayori, M. Hamamoto, et al. 2005. Function of sigma$_1$ receptors in Parkinson's disease. *Acta Neurol. Scand.* 112:103–107. http://dx.doi.org/10.1111/j.1600-0404.2005.00432.x

Mishina, M., M. Ohyama, K. Ishii, S. Kitamura, Y. Kimura, K. Oda, K. Kawamura, T. Sasaki, S. Kobayashi, Y. Katayama, and K. Ishiwata. 2008. Low density of sigma1 receptors in early Alzheimer's disease. *Ann. Nucl. Med.* 22:151–156. http://dx.doi.org/10.1007/s12149-007-0094-z

Monnet, F.P. 2005. Sigma-1 receptor as regulator of neuronal intracellular Ca^{2+}: clinical and therapeutic relevance. *Biol. Cell.* 97:873–883. http://dx.doi .org/10.1042/BC20040149

Mori, T., T. Hayashi, E. Hayashi, and T.-P. Su. 2013. Sigma-1 receptor chaperone at the ER-mitochondrion interface mediates the mitochondrion-ER-nucleus signaling for cellular survival. *PLoS One.* 8:e76941. http://dx.doi .org/10.1371/journal.pone.0076941

Muik, M., M. Fahrner, I. Derler, R. Schindl, J. Bergsmann, I. Frischauf, K. Groschner, and C. Romanin. 2009. A cytosolic homomerization and a modulatory domain within STIM1 C terminus determine coupling to ORAI1 channels. *J. Biol. Chem.* 284:8421–8426. http://dx.doi.org/10 .1074/jbc.C800229200

Navarro, J.F., D. Beltrán, and M. Cavas. 2012. Effects of (+) SKF 10,047, a sigma-1 receptor agonist, on anxiety, tested in two laboratory models in mice. *Psicothema.* 24:427–430.

Ono, Y., H. Tanaka, M. Takata, Y. Nagahara, Y. Noda, K. Tsuruma, M. Shimazawa, I. Hozumi, and H. Hara. 2014. SA4503, a sigma-1 receptor agonist, suppresses motor neuron damage in in vitro and in vivo amyotrophic lateral sclerosis models. *Neurosci. Lett.* 559:174–178. http://dx.doi.org /10.1016/j.neulet.2013.12.005

Pabba, M. 2013. The essential roles of protein-protein interaction in sigma-1 receptor functions. *Front. Cell. Neurosci.* 7:50. http://dx.doi.org/10.3389 /fncel.2013.00050

Palmer, C.P., R. Mahen, E. Schnell, M.B.A. Djamgoz, and E. Aydar. 2007. Sigma-1 receptors bind cholesterol and remodel lipid rafts in breast cancer cell lines. *Cancer Res.* 67:11166–11175. http://dx.doi.org/10.1158 /0008-5472.CAN-07-1771

Palty, R., A. Raveh, I. Kaminsky, R. Meller, and E. Reuveny. 2012. SARAF inactivates the store operated calcium entry machinery to prevent excess calcium refilling. *Cell.* 149:425–438. http://dx.doi.org/10.1016/j.cell .2012.01.055

Parekh, A.B., and J.W. Putney Jr. 2005. Store-operated calcium channels. *Physiol. Rev.* 85:757–810. http://dx.doi.org/10.1152/physrev.00057.2003

Park, C.Y., P.J. Hoover, F.M. Mullins, P. Bachhawat, E.D. Covington, S. Raunser, T. Walz, K.C. Garcia, R.E. Dolmetsch, and R.S. Lewis. 2009. STIM1 clusters and activates CRAC channels via direct binding of a cytosolic domain to Orai1. *Cell.* 136:876–890. http://dx.doi.org/10.1016/j.cell.2009.02.014

Park, C.Y., A. Shcheglovitov, and R. Dolmetsch. 2010. The CRAC channel activator STIM1 binds and inhibits L-type voltage-gated calcium channels. *Science.* 330:101–105. http://dx.doi.org/10.1126/science.1191027

Prakriya, M., S. Feske, Y. Gwack, S. Srikanth, A. Rao, and P.G. Hogan. 2006. Orai1 is an essential pore subunit of the CRAC channel. *Nature.* 443:230–233. http://dx.doi.org/10.1038/nature05122

Rizzuto, R., D. De Stefani, A. Raffaello, and C. Mammucari. 2012. Mitochondria as sensors and regulators of calcium signalling. *Nat. Rev. Mol. Cell Biol.* 13:566–578. http://dx.doi.org/10.1038/nrm3412

Robson, M.J., B. Noorbakhsh, M.J. Seminerio, and R.R. Matsumoto. 2012. Sigma-1 receptors: Potential targets for the treatment of substance abuse. *Curr. Pharm. Des.* 18:902–919. http://dx.doi.org/10.2174/138161212799436601

Sabino, V., P. Cottone, S.L. Parylak, L. Steardo, and E.P. Zorrilla. 2009. Sigma-1 receptor knockout mice display a depressive-like phenotype. *Behav. Brain Res.* 198:472–476. http://dx.doi.org/10.1016/j.bbr.2008.11.036

Schäuble, N., S. Lang, M. Jung, S. Cappel, S. Schorr, Ö. Ulucan, J. Linxweiler, J. Dudek, R. Blum, V. Helms, et al. 2012. BiP-mediated closing of the Sec61 channel limits Ca^{2+} leakage from the ER. *EMBO J.* 31:3282–3296. http://dx.doi.org/10.1038/emboj.2012.189

Skuza, G., and Z. Rogóz. 2006. Effect of BD 1047, a sigma$_1$ receptor antagonist, in the animal models predictive of antipsychotic activity. *Pharmacol. Rep.* 58:626–635.

Soboloff, J., B.S. Rothberg, M. Madesh, and D.L. Gill. 2012. STIM proteins: dynamic calcium signal transducers. *Nat. Rev. Mol. Cell Biol.* 13:549–565. http://dx.doi.org/10.1038/nrm3414

Spruce, B.A., L.A. Campbell, N. McTavish, M.A. Cooper, M.V.L. Appleyard, M. O'Neill, J. Howie, J. Samson, S. Watt, K. Murray, et al. 2004. Small molecule antagonists of the sigma-1 receptor cause selective release of the death program in tumor and self-reliant cells and inhibit tumor growth in vitro and in vivo. *Cancer Res.* 64:4875–4886. http://dx.doi.org/10.1158/0008-5472.CAN-03-3180

Srikanth, S., and Y. Gwack. 2012. Orai1, STIM1, and their associating partners. *J. Physiol.* 590:4169–4177. http://dx.doi.org/10.1113/jphysiol.2012.231522

Srikanth, S., and Y. Gwack. 2013. Molecular regulation of the pore component of CRAC channels, Orai1. *Curr. Top. Membr.* 71:181–207. http://dx.doi.org/10.1016/B978-0-12-407870-3.00008-1

Srikanth, S., H.J. Jung, K.D. Kim, P. Souda, J. Whitelegge, and Y. Gwack. 2010. A novel EF-hand protein, CRACR2A, is a cytosolic Ca^{2+} sensor that stabilizes CRAC channels in T cells. *Nat. Cell Biol.* 12:436–446. http://dx.doi.org/10.1038/ncb2045

Srikanth, S., M. Jew, K.D. Kim, M.K. Yee, J. Abramson, and Y. Gwack. 2012. Junctate is a Ca^{2+}-sensing structural component of Orai1 and stromal interaction molecule 1 (STIM1). *Proc. Natl. Acad. Sci. USA.* 109:8682–8687. http://dx.doi.org/10.1073/pnas.1200667109

Srikanth, S., B. Ribalet, and Y. Gwack. 2013. Regulation of CRAC channels by protein interactions and post-translational modification. *Channels (Austin).* 7:354–363. http://dx.doi.org/10.4161/chan.23801

Stone, J.M., E. Årstad, K. Erlandsson, R.N. Waterhouse, P.J. Ell, and L.S. Pilowsky. 2006. [^{123}I]TPCNE—a novel SPET tracer for the sigma-1 receptor: first human studies and in vivo haloperidol challenge. *Synapse.* 60:109–117. http://dx.doi.org/10.1002/syn.2028116715498

Su, T.-P., T. Hayashi, T. Maurice, S. Buch, and A.E. Ruoho. 2010. The sigma-1 receptor chaperone as an inter-organelle signaling modulator. *Trends Pharmacol. Sci.* 31:557–566. http://dx.doi.org/10.1016/j.tips.2010.08.007

Tchedre, K.T., R.-Q. Huang, A. Dibas, R.R. Krishnamoorthy, G.H. Dillon, and T. Yorio. 2008. Sigma-1 receptor regulation of voltage-gated calcium channels involves a direct interaction. *Invest. Ophthalmol. Vis. Sci.* 49:4993–5002. http://dx.doi.org/10.1167/iovs.08-1867

Tsai, S.Y.A., M.J. Pokrass, N.R. Klauer, N.E. De Credico, and T.-P. Su. 2014. Sigma-1 receptor chaperones in neurodegenerative and psychiatric disorders. *Expert Opin. Ther. Targets.* 18:1461–1476. http://dx.doi.org/10.1517/14728222.2014.972939

van Waarde, A., A.A. Rybczynska, N.K. Ramakrishnan, K. Ishiwata, P.H. Elsinga, and R.A.J.O. Dierckx. 2015. Potential applications for sigma receptor ligands in cancer diagnosis and therapy. *Biochim. Biophys. Acta.* 1848:2703–2714. http://dx.doi.org/10.1016/j.bbamem.2014.08.022

Várnai, P., B. Tóth, D.J. Tóth, L. Hunyady, and T. Balla. 2007. Visualization and manipulation of plasma membrane-endoplasmic reticulum contact sites indicates the presence of additional molecular components within the STIM1-Orai1 complex. *J. Biol. Chem.* 282:29678–29690. http://dx.doi.org/10.1074/jbc.M704339200

Vilner, B.J., C.S. John, and W.D. Bowen. 1995. Sigma-1 and sigma-2 receptors are expressed in a wide variety of human and rodent tumor cell lines. *Cancer Res.* 55:408–413.

Walker, J.M., W.D. Bowen, F.O. Walker, R.R. Matsumoto, B. De Costa, and K.C. Rice. 1990. Sigma receptors: biology and function. *Pharmacol. Rev.* 42:355–402.

Wang, B., R. Rouzier, C.T. Albarracin, A. Sahin, P. Wagner, Y. Yang, T.L. Smith, F. Meric-Bernstam, C. Marcelo Aldaz, G.N. Hortobagyi, and L. Pusztai. 2004. Expression of sigma 1 receptor in human breast cancer. *Breast Cancer Res. Treat.* 87:205–214. http://dx.doi.org/10.1007/s10549-004-6590-0

Wang, L., A.R. Prescott, B.A. Spruce, J. Sanderson, and G. Duncan. 2005. Sigma receptor antagonists inhibit human lens cell growth and induce pigmentation. *Invest. Ophthalmol. Vis. Sci.* 46:1403–1408. http://dx.doi.org/10.1167/iovs.04-1209

Wang, Y., X. Deng, S. Mancarella, E. Hendron, S. Eguchi, J. Soboloff, X.D. Tang, and D.L. Gill. 2010. The calcium store sensor, STIM1, reciprocally controls Orai and CaV1.2 channels. *Science.* 330:105–109. http://dx.doi.org/10.1126/science.1191086

Waterhouse, R.N., R.C. Chang, N. Atuehene, and T.L. Collier. 2007. In vitro and in vivo binding of neuroactive steroids to the sigma-1 receptor as measured with the positron emission tomography radioligand [^{18}F]FPS. *Synapse.* 61:540–546. http://dx.doi.org/10.1002/syn.2036917447254

Willoughby, D., K.L. Everett, M.L. Halls, J. Pacheco, P. Skroblin, L. Vaca, E. Klussmann, and D.M.F. Cooper. 2012. Direct binding between Orai1 and AC8 mediates dynamic interplay between Ca^{2+} and cAMP signaling. *Sci. Signal.* 5:ra29. http://dx.doi.org/10.1126/scisignal.2002299

Wu, Z., and W.D. Bowen. 2008. Role of sigma-1 receptor C-terminal segment in inositol 1,4,5-trisphosphate receptor activation: constitutive enhancement of calcium signaling in MCF-7 tumor cells. *J. Biol. Chem.* 283:28198–28215. http://dx.doi.org/10.1074/jbc.M802099200

Wu, M.M., E.D. Covington, and R.S. Lewis. 2014. Single-molecule analysis of diffusion and trapping of STIM1 and Orai1 at endoplasmic reticulum-plasma membrane junctions. *Mol. Biol. Cell.* 25:3672–3685. http://dx.doi.org/10.1091/mbc.E14-06-1107

Wünsch, B. 2012. The σ_1 receptor antagonist S1RA is a promising candidate for the treatment of neurogenic pain. *J. Med. Chem.* 55:8209–8210. http://dx.doi.org/10.1021/jm3011993

Xu, X.J., M. Boumechache, L.E. Robinson, V. Marschall, D.C. Gorecki, M. Masin, and R.D. Murrell-Lagnado. 2012. Splice variants of the P2X7 receptor reveal differential agonist dependence and functional coupling with pannexin-1. *J. Cell Sci.* 125:3776–3789. http://dx.doi.org/10.1242/jcs.099374

Yamamoto, H., J. Karasawa, N. Sagi, S. Takahashi, K. Horikomi, S. Okuyama, T. Nukada, I. Sora, and T. Yamamoto. 2001. Multiple pathways of σ_1 receptor ligand uptakes into primary cultured neuronal cells. *Eur. J. Pharmacol.* 425:1–9. http://dx.doi.org/10.1016/S0014-2999(01)01143-8

Yuan, J.P., W. Zeng, M.R. Dorwart, Y.J. Choi, P.F. Worley, and S. Muallem. 2009. SOAR and the polybasic STIM1 domains gate and regulate Orai channels. *Nat. Cell Biol.* 11:337–343. http://dx.doi.org/10.1038/ncb1842